Corresponding address: Centre for Earth Evolution and Dynamics (CEED), Department of Geosciences, University of Oslo, PO Box 1028, N-0315 Oslo, Norway

Crustal structure and erosion of the Lofoten/Vesterålen shelf, northern Norwegian margin

Asbjørn Johan Breivik[a,], Jan Inge Faleide[a], Rolf Mjelde[b], Ernst R. Flueh[c], Yoshio Murai[d]

[a]*Centre for Earth Evolution and Dynamics (CEED), Department of Geosciences, University of Oslo, Norway*
[b]*Department of Earth Science, University of Bergen, Norway*
[c]*GEOMAR Helmholtz Centre for Ocean Research Kiel, Germany*
[d]*Institute of Seismology and Volcanology, Faculty of Science, Hokkaido University, Sapporo, Japan*

Abstract

The Norwegian continental shelf has been through several rift phases since the Caledonian orogeny. Early Cretaceous rifting created the largest sedimentary basins, and Early Cenozoic continental breakup between East Greenland and Europe affected the continental shelf to various degrees. The Lofoten/Vesterålen shelf is located off Northern Norway, bordering the epicontinental Barents Sea to the northeast, and the deep-water Lofoten Basin to the west. An ocean bottom seismometer/hydrophone (OBS) survey was conducted over the shelf and margin areas in 2003 to constrain crustal structure and margin development. This study presents Profile 8-03, located between the islands of Lofoten/Vesterålen and the shelf edge. The wide-angle seismic data were modeled using forward/inverse raytracing to build a crustal velocity-depth transect. Gravity modeling was used to resolve an ambiguity in seismic Moho identification in the southwestern part. Results show a crustal thickness of $\sim$31 km, significantly thicker than what a vintage land station based study suggested. Profile 8-03 and other OBS profiles to the southwest show high sedimentary velocities at or near the seafloor, increasing rapidly with depth. Sedimentary velocities were compared to the velocity-depth function derived from an OBS profile at the Barents Sea margin, tied to a coincident well log, where there is little erosion. Results from this profile and the crossing Profile 6-03 (Breivik et al., 2017) indicate three major erosion episodes; Late Triassic-Early Jurassic, tentatively mid-Cretaceous, Late Cretaceous-early Cenozoic, and a minor late glacial erosion

episode off Vesterålen.

Key words: Ocean bottom seismometers, Gravity, Crustal structure, Erosion, Norwegian shelf

1. Introduction

The Lofoten/Vesterålen shelf is narrow and part of the Norwegian shelf that borders the epicontinental Barents Sea to the north (Fig.1). It is located off the islands of Lofoten in the south, and the islands of Vesterålen in the north. Onshore rocks on these islands consist mostly of high-grade Archean to Proterozoic complexes (e.g., Griffin et al., 1978). The area shows little Caledonian overprint, despite being located within the main continental collision zone. This has been attributed to the area having a strong crust due to a dominantly dry and granulitic composition (e.g., Ormaasen, 1977; Griffin et al., 1978; Schlinger, 1985).

Later development comprises rift events from the Permian-Triassic to the Eocene, as seen at other parts of the Norwegian shelf, where the Early Cretaceous rifting appears to be the strongest (e.g., Hansen et al., 2012). However, the shelf area has sedimentary basins 5-6 km deep at most in our study area (e.g., Løseth and Tveten, 1996), and basement outcrops locally in the Utrøst Ridge (Mjelde et al., 1992; Hansen et al., 2012; Breivik et al., 2017). Thus, the shelf area appears resistant to the extensional events which produced sedimentary basins in excess of 15 km deep on the Møre Marin/Vøring Plateau and in the Barents Sea (e.g., Mjelde et al., 1993, 1997, 2005; Breivik et al., 1998; Faleide et al., 2008; Osmundsen and Ebbing, 2008). The sedimentary strata on the shelf within our study area are mostly of Cretaceous age (e.g., Hansen et al., 2012; Tasrianto and Escalona, 2015). A thin section of Jurassic strata as well as older sedimentary layers may be present in some parts. The last major extensional phase occurred during continental breakup from the latest Cretaceous through the earliest Eocene, creating rotated fault blocks and much of the present structure. Truncation of sedimentary strata in these fault blocks (e.g., Hansen et al., 2012) shows that there has been substantial later erosion of the shelf, though there are few erosion estimates based on quantitative methods for the area.

Email addresses: a.j.breivik@geo.uio.no (Asbjørn Johan Breivik)

Only two earlier wide-angle seismic studies covering the Lofoten/Vesterålen shelf have been conducted (Fig.1). The oldest one was collected during a field campaign in the late 1960s to early 1970s (Sellevoll, 1983). It used land-based receivers deployed in a crooked line geometry defining a ∼150 km long seismic model, with explosive sources off each end deployed in shallow sea. The result of this experiment has been a long-standing reference to the crustal structure of the shelf west of Lofoten/Vesterålen. It suggested a fairly thin crust with a Moho depth of 21-26 km, shallowest in the south. The newer profile was collected in 1988 across the southern part of Lofoten, and used ocean bottom seismometers and a marine airgun source (Mjelde et al., 1993). The 175 km long model shows the shallowest Moho depth of about 20 km under the southernmost part of Lofoten. Farther west, the Moho depth increases to about 27 km underneath the southern Utrøst Ridge near the shelf edge, to become shallower towards the outer margin again.

The profile presented here (Profile 8-03) is part of a larger regional OBS survey (Euromargins 2003), deploying OBSs and a few land stations, using marine airgun shots (Fig.1). From this survey, Profile 6-03 crossing the inner part of Lofoten was recently published (Breivik et al., 2017). It shows a crustal structure very different from that of the older models, with a Moho depth of ∼36 km beneath the inner part of Lofoten. Profile 8-03 crosses this profile and is located about midway between the islands and the shelf edge, sub-parallel to and 10-30 km west of the Sellevoll (1983) profile (Fig.1). We will take a closer look at the constraints this profile give on the crustal structure of the outer shelf, by combined use of the seismic data and the shipboard recorded gravity, and discuss the reasons why the newer survey gives such different results compared to vintage studies. The shelf area is affected by several phases of erosion (e.g., Løseth and Tveten, 1996). Both Profiles 6-03 and 8-03 give good constraints on the sedimentary velocities for central parts of the shelf, and we also present erosion estimates based on the relationship between burial depth and velocity, by comparing to coincident OBS and well data from the Barents Sea. This can be related to vertical movement of the area in general, but will also have implications for assessing the petroleum potential of the area (e.g., Ohm et al., 2008; Baig et al., 2016).

2. Data Acquisition and Processing

The survey took place during the summer of 2003 by use of the R/V Håkon Mosby, involving the Norwegian Department of Geosciences, University of Oslo, and the Department of Earth Science, University of Bergen, in collaboration with GEOMAR, Kiel, Germany, and the Institute for Seismology and Volcanology (ISV), Hokkaido University, Sapporo, Japan. The seismic source consisted of four equal-sized air guns in an array with a total volume of 78.66 L (4800 in^3), fired at 200 m intervals and towed at 12 m depth, using an air pressure of approx. 140 bar. Two types of ocean bottom seismometers were used to record the seismic arrivals. The ISV OBSs have three orthogonally mounted components with analog or digital recording. The GEOMAR instruments use digital recording and have three orthogonally mounted components and a hydrophone, or a single hydrophone only. The latter is abbreviated OBH when specifically identified, otherwise OBS is used as a general term. Navigation used Differential Global Positioning System (GPS) readings. The shot line is 205 km long with eleven instruments deployed, where nine recorded useful data (Fig.1).

Pre-processing consisted of first adjusting for clock drift, after which a 60 s record length was extracted for each shot, and then tied to navigation. The instrument positions on the seafloor along profile were corrected from the drop point to account for current drift, estimated from the timing of the water arrival. Initial processing included de-biasing, bandpass filtering (6-12 Hz), and offset dependent scaling. A second processing flow including spiking deconvolution was then used for comparison, where secondary arrivals can be easier to interpret. All seismic examples shown here are based on this latter sequence, applying a velocity reduction of 8 km s^{-1}. The processing was done with Seismic Unix. The ship Echo sounding data was used to constrain seafloor depth along profile.

Gravity was recorded at 10 s intervals by a LaCoste & Romberg S-99 gravimeter mounted on a stabilized platform. Port measurements in Bergen were used to correct for instrumental drift, and absolute gravity was established by tying to a reference point at the University of Bergen. The gravimeter has a 60 point internal smoothing filter, so the logged value was repositioned to the middle of the filter (300 s earlier) using the ship navigation. The data went through a standard processing sequence including latitude and Eötvös corrections based on the navigation, to produce Free-Air gravity. The Eötvös correction was similarly smoothed over the same time interval (10 min.) as the gravity readings. At the end, short-wavelength noise was removed by applying a 5 km wide Gaussian spatial filter from the GMT software (Wessel and Smith, 1991; Wessel et al., 2013).

3. Methods

The travel time for different arrivals are interpreted from each OBS/OBH data set, and modeled with the raytracing software Rayinvr (Zelt and Smith, 1992). The program also has node-specific inversion functionality which is useful for finding the best solutions, and for deriving resolution statistics. However, inversion results may have to be modified in order to improve the ability of the model to trace rays to all observed offsets. An important part of the process is to identify seismic phases, which comprise groups of seismic arrivals that travel a similar direction through the model, and thus can constrain specific features in the underground. Arrivals with increasing travel times are fit from top and downwards layer by layer, building the model iteratively.

Interpretation of arrival times has some uncertainty to it due to noise, and additional issues arising from inaccuracies in instrument location (especially off-line), bathymetry, and shot timing. Noise can make it difficult to pick the first onset of an arrival, and the pick uncertainty is estimated to have an error of approximately $\pm$ the width of one cycle, and is the main contribution in this study. Rayinvr will use this given interpretation uncertainty to estimate the goodness of fit between observed and calculated travel times from the model. It is using χ^2 statistical analysis, where a value of 1 or lower shows a fit within the estimated interpretation uncertainty. Short offset arrivals traveling through sedimentary layers are estimated to $\pm$50 ms, basement arrivals are given $\pm$75-100 ms, while clear Moho arrivals are given an uncertainty of $\pm$100 ms. Up to $\pm$150 ms uncertainty was used for some weak arrivals.

The Rayinvr program package offers the option to export a polygon-based density model based on an empirical relationship between velocity and density (Bezada and Zelt, 2011). It will use each trapezoid defining the velocity model, find the average velocity within each, and convert that to a density. The trapezoids and the estimated densities will then define a polygon for use in 2D forward gravity response modeling based on the algorithm of Talwani et al. (1959). Thus, the significance of a velocity model change can quickly be tested for its gravity response, which can be useful if there are ambiguities in the phase identification in the seismic data. In order to reduce edge effects, the model is extrapolated one model width to each side when exported from Rayinvr. However, this extrapolation is on the low side to completely eliminate them. Therefore a density of 2900 kg m^{-3} is subtracted from all polygon densities before calculation to reduce the density contrast of the model to the zero density existing beyond its ends. Since the gravity response of the model is only dependent on lateral density contrasts, this further reduces the edge effect of the model. The subtracted density is estimated to be close to the average density of the crustal and upper mantle polygons. Changing this value by $\pm$100 kg m^{-3} affects the calculated gravity response at the ends of the model by less than 1 mGal.

The last method that will be applied to the results of the modeling uses the relationship between sediment burial, compaction and diagenesis, and the seismic velocities of sedimentary rocks (e.g., Nafe and Drake, 1957). The general velocity increase with burial depth has been exploited in many settings to make erosion estimates based on the current velocity-depth trends (e.g., Heasler and Kharitonova, 1996; Baig et al., 2016). In order to do that, we establish a range of velocity-depth curves from a non-eroded part of the western Barents Sea margin, based on the results of an OBS profile (Mjelde et al., 2002), which can be compared to a coincident well log (Ryseth et al., 2003) (Fig. 1).

4. P-Wave Modeling

The OBS Profile 8-03 was shot along an older (1986) multi-channel reflection profile (Fig. 1). It is of moderate quality, and has not previously been published (Fig. 2). In the southwest there is a strong and continuous reflection at 1-2 seconds depth outlining a basin, and published crossing lines indicate that this reflector represents Base Cretaceous (Tsikalas et al., 2001; Hansen et al., 2012). According to the crossing lines, there could be a thin layer of Upper or Middle Jurassic strata present below this level also, resting on basement. The basin belongs to the northern part of the Ribban Basin, here called the Havbåen Subbasin. A similar reflection can be followed to the northeast for most of the profile, but is missing below Bleiksdjupet. Here there is a clearer layering to the upper sedimentary part, apparently of Cenozoic age (e.g., Bergh et al., 2007; Tasrianto and Escalona, 2015). This profile was used to guide a starting model, but the subsequent travel-time modeling ultimately decided the number of sedimentary layers needed, as well as the variation in depth to the top of each of them and to the top of the basement. Likewise, the number of layers used for the crystalline crust is determined by the data only, and not by tie to the crossing Profile 6-03 (Breivik et al., 2017).

4.1. Data Constraints

Two OBSs located at the northeastern end of the profile did not record any data, reducing the model constraints there (Fig. 1). Of the remaining nine stations (Figs. 3-9), two instruments (OBS 85 and OBH 84) did not record much more than short-offset sedimentary arrivals. Five stations (OBSs 89, 88, 67, 87, and 83) recorded arrivals down to the Moho, providing crustal thickness control. Data quality is in general very good in the southwest (OBSs 89, 88, 67, 87), while it is more variable for stations located at the central and northeastern parts of the profile.

Starting in the southwest, OBS 90 provided a data set with good amplitude on lower-crustal arrivals observed up to almost 200 km offset (Fig. 3). Arrivals that give modeled velocities in the 6.0-6.2 km s^{-1} range are typical for crystalline crust in the area (Chroston and Brooks, 1989), and were used to interpret the top of the basement. It is at the most shallow ($\sim$2 km depth) at the eastern edge of the Utrøst Ridge, called Jennegga High here (Fig. 10). It deepens to about 6 km to the northeast in the Havbåen Subbasin (Northern Ribban Basin), but basement shoals again to between 2 and 3 km depth, limiting this subbasin to between 15 and 60 km in the model. Top basement refractions are hard to trace as diving waves to all observed locations here due to the dipping top basement topography, a relatively thin upper crustal layer, and a low velocity gradient, and was therefore modeled as headwaves. There are both upper- and lower-crustal refractions and reflections with good amplitude. The lower reflection appears to originate at around 26 km depth, a level that is also used to model reflectivity on OBS 87 from the opposite direction (Fig. 7). At that depth it could potentially be a Moho reflection (P$_M$P), though this is shallower than the $\sim$31 km depth seen in central parts of the profile. There is no upper-mantle refracted arrivals (P$_n$) tied to this level here, so it cannot be securely identified as the Moho. The phase identification was further tested by gravity modeling (described below), which supports a lower-crustal reflector origin. However, this was not easily tied to the velocity layering of the model, and therefore modeled by a floating reflector.

The neighboring OBS 89 has a similar data quality (Fig. 4). Top basement had to be modeled by headwaves also here. A late incoming high amplitude reflection is observed between 130 and 180 km in the data. This was modeled as a P_MP phase originating at ∼31 km depth between 80 and 100 km in the model. A short P_n phase, requiring a typical upper mantle velocity of 7.95 km s^{-1}, can be seen at the northeastern end of the seismic panel, confirming the Moho level. It enters the mantle near 70 km in the model and leaves between approx. 155 and 160 km. Other OBSs show similar reflections partly overlapping this area of the Moho, up to 130 km in the model. The most important of these is OBS 88, the only other data set that shows a P_n phase tied to this level (Fig. 5). The P_n phase is clearer, and enters the mantle near 90 km in the model, and leaves between approx. 150 and 165 km, fitting the same 7.95 km s^{-1} velocity. These two OBSs constrain upper, middle, and lower crustal levels towards central and northeastern parts of the transect. To the southwest of the OBS location, the top basement arrivals were modeled using headwaves, while deeper levels only show some reflections.

OBSs located in the central parts of the model do not show refractions from the lower crust, probably due to less shot-receiver offset distance on both sides. The first of these is OBS 67, where top basement arrivals were modeled by headwaves at offsets up to approx. 100 km (Fig. 6). First arrivals at greater offsets were modeled as diving waves in the middle crustal layer towards the northeast. A quite strong P_MP phase originated from between 110 and 130 km at the Moho. The adjacent OBS 87 data show top basement arrivals that were modeled by headwaves near the instrument, and by diving waves up to 70 km offset (Fig. 7). Refracted arrivals at offsets greater than this on both sides had to be traced through the middle crustal layer. This data set also shows a lower-crustal reflection that fits with the floating reflector introduced for OBS 90, but from the opposite direction. OBS 87 data also show a somewhat indistinct Moho reflection consistent with that of OBS 88 (Fig. 5).

Data quality is in general poorer for the northeastern instruments. OBH 86 (Fig. 8) gives similar constraints on the upper and middle crust as OBS 87 (Fig. 7) to the southwest of it. However, the signal-to-noise ratio is lower, and there are sections where no arrivals could be identified (Fig. 8). OBS 85 to the northeast mostly shows refracted arrivals from the sedimentary layers, and a weak arrival at 60 to 80 km offset, modeled as diving waves through the top basement (Fig. 8). The adjacent OBH 84 shows refracted arrivals through the sedimentary part only (Fig. 9). The north-easternmost OBS 83 has better data quality, though not quite on par with the southwestern group of instruments (Fig. 9). Towards the southwest, the top basement arrival was modeled as a headwave up to 70 km offset. At greater offsets, the data set provides reverse shot coverage of refractions from middle and lower crustal layers in central parts of the model, as well as a P_MP phase reflecting from the same area of the Moho covered from the OBSs in the southwestern part. Arrivals to the northeast of the instrument are present only at short offsets, up to approx. 20 km, and thus provide little information about the crust below the sedimentary section here.

4.2. Modeling Results

A gridded display of the velocity model is shown in Figure 10. The total thickness of the sedimentary layers vary between 1.5 and 6.5 km. It is greatest in the Havbåen Subbasin in the southwest, and at the northeastern end of the profile off Vesterålen, at the southern margin of the Harstad Basin. There is a decrease of sedimentary rock velocity from the southwest to the northeast. This is particularly apparent at or near the seafloor, where velocities range from 3.1 to 3.5 km s^{-1} in the central and southwestern parts, but a new layer appears at the seafloor in the northeast. That layer is thin in the center of the model, but increases up 1.2 km in the northeast. Velocities in the top of this layer are variable, ranging from 1.8 km s^{-1} in the center of the model, to 2.2 km s^{-1} around Bleiksdjupet (also called the Andøya Canyon) (e.g., Rise et al., 2013) in the northeast. This layer is apparently of Cenozoic age. The layer below, that is also exposed at the seafloor in the southwest, is of Upper Cretaceous age (e.g., Hansen et al., 2012). In the Havbåen Subbasin, the lower layer should be of Lower Cretaceous age, but it is not clear how it continues to the northeast. There appears to be a fault zone at the edge of the basin, though it is not clear in the reflection seismic profile how it displaces deeper sedimentary layers (Fig. 2). The Upper Cretaceous layer is thicker to the northeast, and the layer below appears to be Lower Cretaceous, but with higher velocities than in the Havbåen Subbasin. The lowermost sedimentary layer in the Havbåen Subbasin is poorly imaged in the reflection seismic profile, though there are some discontinuous reflections below the Base Cretaceous reflector. It most likely consists of Upper Paleozoic to Jurassic sedimentary rocks.

Upper crystalline basement velocities lie mostly between 6.0 to 6.3 km s^{-1}, except for at the northeastern end where it drops to a less well-constrained 5.8 km s^{-1}. However, preliminary results from the crossing Profile 5-03 support this velocity at the tie. Since the velocity is at the low end of what is expected for crystalline rocks, it could also represent well-consolidated Paleozoic sedimentary rocks. Velocities are around 6.0 km s^{-1} in central parts of the profile where basement is the shallowest. The middle crustal layer has slightly higher velocities, ranging from 6.35 to 6.65 km s^{-1}, highest in an area around 130 km in the model. There is a distinct increase in velocity to the lower crust, which shows velocities of 6.85 km s^{-1} in the top, increasing to $\sim$7 km s^{-1} at the bottom. OBSs 67, 87 and 88 show strong reflections that can be tied to the top of this layer, some of them originating near the tie to the crossing Profile 6-03 (Breivik et al., 2017). On that profile, the top of the layer also gave strong reflections.

Moho depth is seismically constrained between 70 and 165 km in the model, varying from 30.8 to 31.3 km. It is constrained by P_MP phases, combined with two P_n phases seen on OBSs 88 and 89 (Figs. 4, 5), giving a top mantle velocity of 7.95 km s^{-1}. This level fits with the tie to Profile 6-03 crossing the model at $\sim$70 km (Breivik et al., 2017). The gravity modeling described below requires that this level should not change southwestwards towards the end of the model. The shoaling at the northeastern end was indicated by the gravity modeling, but not constrained by seismic data here. The other crossing profiles are not yet finalized, but have too little overlap to provide information about crustal thickness at the ties due to the deep-crustal shadow zones at the model ends.

Profiles 8-03 and 6-03 were modeled semi-independently from each other. Figure 11 shows 1D velocity functions from each at the tie. Moho depth and lower crustal velocity were coordinated between the profiles. Only Profile 8-03 constrained the lower crustal velocity, and contributed this to Profile 6-03 (Breivik et al., 2017). However, Profile 6-03 crossed several crustal domains with rapid changes along the model, and required more layers within the crystalline crust than Profile 8-03 to reproduce the different phases. To make a perfect tie here would have introduced complexity to the Profile 8-03 model that is not supported by the data. Still the velocities of the upper crystalline crust of the models are quite similar, but slightly lower at Profile 8-03. The discrepancy could be related both to modeling uncertainty, and to lateral variations within the orthogonally oriented profiles away from the tie. Anisotropy can sometimes be present, but the results are probably not well enough constrained to support any conclusions about that here. Similarly, there are some differences in the sedimentary section. The high sedimentary velocities at the seafloor are practically identical at 3.5 km s^{-1}. The top of the next layer shows more difference, 4.5-4.8 km s^{-1}, again slightly lower at Profile 8-03. This may be due to the structurally complexity at the edge of the basin, with a normal fault through the area on Profile 8-03.

4.3. Model Coverage and Resolution

The fit statistics for the refracted phases and Moho reflections are shown in Table 1. The fit is somewhat poorer where arrivals could only be traced as head waves due to the model geometry. The ray coverage density is shown in Figure 12A. The top basement is best covered in central and southwestern parts, while the middle basement level has the highest ray density in central and northeastern parts. Lower crust as well as the Moho is best covered in the central part.

Another way of looking at the quality of constraints for individual nodes is to examine the diagonal values of the resolution matrix obtained from the inversion tool in Rayinvr. That will show how independent individual nodes are from their neighbors. Values can be between 0 and 1, and if above 0.5 it indicates a reasonably well resolved parameter (Zelt and Smith, 1992). The grid of Figure 12B was created by inverting velocity while holding the geometry fixed (using a damping factor of 1). Only refracted phases were included, since reflections do not put strong constraints on velocity. Figure 12B shows that the velocity of the sedimentary layers at or near the seafloor is well constrained. The lower sedimentary layer is also reasonably well constrained, but less than the shallower. The weakest constraints are to the northeast where data coverage is low, and below OBH 84 and OBS 85, which also are the poorest data sets. Deeper down, there is a good correlation with the ray coverage shown in Figure 12A. Top basement velocity is best constrained in central and southwestern parts of the model, but still good in the northeast. Middle basement level velocity resolution is good in central parts. The lower crust has less ray coverage and poorer resolution of the velocity nodes towards the model ends. The bottom velocity of the lower crustal layer is less well constrained. Top mantle velocity is well constrained only in a small area in central parts, between 100 and 125 km in the model.

To estimate the depth node resolution the velocity was held constant, while depth nodes were similarly inverted for using both refractions and reflections. Top crystalline basement, as well as the two internal basement layer interfaces and the Moho were tested. The size of the circles enclosing the depth nodes indicates the resolution (Fig. 12B). Top basement depth is well constrained along the model. The resolution is also good for the deeper crustal layers and Moho, though increasingly poor at the ends as the depth increases. The Moho is well resolved between 80 and 160 km in the model. However, the resolution statistics do not directly quantify error bounds.

Since sedimentary velocities will be used in the erosion estimates, the velocity uncertainty that is allowable within a χ^2 value less than 1 was determined from the phases constraining these. For the top Cenozoic layer, it is +0.07/-0.05 km s^{-1}. For the top of the Upper Cretaceous layer, it is +0.14/-0.03 km s^{-1}, and for the top of the Lower Cretaceous it is +0.12/-0.05 km s^{-1}.

The thickness of the lower crust constitutes a significant portion of the total crustal thickness, while the velocity is less well constrained than for the upper part of the crystalline crust. The trade-off between bulk lower crustal velocity and Moho depth is therefore investigated, using P$_{g3}$, P$_M$P, and P$_n$ phases. A total of 1271 models were run using an automated procedure, which adjusts depth nodes incrementally in the same direction by 0.1 km steps, while velocity nodes (top and bottom layer) are adjusted incrementally by 0.01 km s^{-1} steps through a given range for each depth iteration. Fit statistics for these models are presented in Figure 13. It appears that the ability to trace rays through the model to all observed locations is quite sensitive to velocity changes. The variable loss of rays results in uneven contours of the χ^2 values, and the Δt fit (RMS time misfit between observed and calculated travel times). Models that fit within the χ^2=1 contour indicate a depth range of the Moho solution of approx. -0.4 km to +0.6 km. However, the models are very sensitive to bulk lower-crustal velocity changes, indicating a range of $\pm$0.03 km s^{-1}.

5. Gravity Modeling

While gravity modeling is inherently non-unique (e.g., Barton, 1986), it can nevertheless provide useful constraints if a clear problem can be formulated. One such problem is the phase identification of strong arrivals seen on OBSs 90 and 87, which could either represent reflections from the lower crust, or alternatively from the Moho. If the latter interpretation was correct, it would mean a shoaling of the Moho from $\sim$31 km in central parts of the profile to approx. 26 km to the southwest.

The gravity field of the shelf reflects known structure well (Fig. 14). The highest gravity anomalies are found in southern Lofoten, while other highs are related to the Utrøst Ridge/Jennegga High, and the outer part of Vesterålen. The Havbåen Subbasin shows as a small circular low under OBS 89 at the southwestern part of the OBS profile. The gravity field variations along Profile 8-03 are moderate (Fig. 15). The Ribban Basin is characterized by positive anomalies with small variations, but these are lower than that of the flanking ridges. The highest gravity is a broad maximum located over the Jennegga High. The lowest gravity is a narrow anomaly over Bleiksdjupet at the northeastern end, reflecting the bathymetry.

The velocity model was converted to density, and the forward gravity response calculated (Fig. 15). There is an overall regional fit between calculated and observed gravity with a fairly flat Moho throughout the profile. The gravity response of Bleiksdjupet is well reproduced, showing that the estimated sedimentary densities are reasonably accurate. On the other hand, the sediment-basement contact has a stronger signature than observed. The top basement is well constrained by the travel time data, indicating that the main reason for this is that the density contrast across the interface is less than estimated from the velocities. The gravity signature of the Havbåen Subbasin in the southwest is reproduced, though the amplitude of the calculated anomaly is somewhat higher than observed. The Moho depth was slightly reduced towards the northeastern end in order to fit the observed gravity level towards the end of the model. The profile is very close to the shelf edge there and some crustal thinning is expected, though this part of the model is not constrained by the seismic data, and no robust conclusions can be drawn.

The main goal of this modeling was to test phase identifications in the southwest. An alternative Moho is shown by the dashed line in the lower crust of the model (Fig. 15), with a corresponding dashed blue line showing the calculated gravity response. Reflections originate at 26 km depth between 40 and 60 km in the model. In the alternative density model, Moho is therefore placed at that level from 20 to 60 km, to correspond approximately to the basin above. This shallow area is tapered down to the original model depth to the southwest. If not, the impact on the calculated gravity would be greater still. The alternative model introduces a regional misfit of $\sim$35 mGal, which does not support a shallower Moho in this region. Therefore, the observed reflections have to come from within the lower crust.

The profile is oriented sub-parallel to the shelf edge, and while there is a change in crustal thickness to the northwest of the profile, it is expected to affect it evenly in a regional sense, and not interfere with the modeling of small-scale features. The part of the profile we tested in the modeling is also located in a region with moderate field variations, parallel to and away from regional highs. In the southwest it terminates in an area with little gravity change. Thus, it is not likely that the conclusion about the Moho depth should be compromised by offline effects.

6. Erosion Estimates

One striking property of the seismic model is the high velocities in the sedimentary section at or near the seafloor, which is also observed at other nearby OBS profiles on the shelf (Breivik et al., 2017; Mjelde et al., 1992, 1993). Velocities are commonly between 3.0 and 3.5 km s^{-1}. This can be compared to results of OBS surveys of the northern Barents Sea where sedimentary rocks at/near seafloor have velocities of 3.3-4.2 km s^{-1} (Breivik et al., 2002, 2005). Erosion is extensive in the Barents Sea, and strongest in the north (Henriksen et al., 2011; Baig et al., 2016) where it may exceed 3 km. There, the Cretaceous section is mostly missing, and erosion usually exposes Triassic strata. The high velocity at/near the seafloor is related to this, as the strata were at one time buried under a significant sedimentary load. The loading causes mechanical compaction as well as diagenetic alteration with increasing depth, which result in an increased seismic velocity. Thus, velocity can be used to estimate the maximum burial and hence amount of erosion. However, the velocity increase with burial is also tied to lithology, and there is uncertainty concerning the choice of reference.

The southwestern Barents Sea margin area appears to have little net erosion, so that the present burial is the maximum depth the sediments have been at there (Baig et al., 2016). In this area there is an exploration well (7216/11-1S) (Ryseth et al., 2003) located almost coincident with an OBS profile (Mjelde et al., 2002). That makes it possible to do a direct comparison between the velocities obtained through the travel-time modeling of wide-angle seismic data (Profile B-98) and a sonic log through the same rocks (Fig. 16). The lithology is primarily mudrock, and should be comparable to the predominantly fine-grained sedimentary succession on the Lofoten/Vesterålen shelf (Hansen et al., 2012). The OBS model divides the upper 4 km into 7 layers, where the velocity in the top of the layers is best constrained, while the velocity gradient is more uncertain. The model was sampled 17 times for 1D velocity profiles at a 2.5 km interval from 10 to 50 model km around the well tie (at $\sim$30 km). This shows some spread to the velocity against depth, probably due to variations in lithology. OBS velocities are slightly higher than the sonic log at the same depth, especially in the shallowest part where it is 0.1-0.3 km s^{-1} above. This is often the case, as wide-angle seismic data sample the faster layers if they are sub-horizontal (e.g., Baig et al., 2016). Therefore, by using an OBS-derived reference, this bias should be reduced. The sonic log shows some high-velocity layers too thin to be detected by the OBS data, tied to carbonates (Ryseth et al., 2003). Between 3 and 4 km depth, the OBS model 1D samples show a rapid velocity increase to about 3.7-4 km s^{-1}. This velocity increase is also seen in the sonic log, tied to a 200-300 m thick zone dominated by Middle Eocene sandstones (Ryseth et al., 2003). The OBS data recorded this layer at 3.4 km depth at the well tie, while the well shows it at about 3 km depth (Fig. 16). Also the velocity inversion below that sequence was not detected in the OBS data. This strong velocity variation over thin layers therefore seems to be smoothed over by the lower resolution of the OBS data, and the reason for the $\sim$400 m depth mismatch at the tie. However, there is a good match with the high-resolution sonic-log velocities down to 3 km, suggesting that the OBS-derived reference velocities can be used for the erosion study down to that depth, but that it will be more uncertain for greater depths.

Two six-order polynomial curves were fitted to the OBS data using least squares, the red using both top and bottom layer points, while the blue uses only the top-layer velocities (Fig. 16). The latter has higher velocities at slightly shallower depth and is more biased towards the sandy layers, though the red curve shows an overall better fit with the sonic log, with a good fit down to a depth of ∼3 km. The velocities of Profile 8-03 can be compared to these two curves, and the maximum burial depth can then be estimated (Fig. 16). Three different levels were analyzed (Fig. 17). For the deeper layers, an erosion event can only be determined if the estimated maximum burial depth exceeds the present burial summed with the estimated erosion on levels above.

First level: The first layer consisting of Cenozoic strata is seen only off Vesterålen, where it is at seafloor. Velocities range from 1.9 to 2.3 km s^{-1}. Erosion may have removed a maximum of 1.2-1.3 km from the top of this layer in the northeast, tapering down to 0 km southwestwards. Including the uncertainty range of the sedimentary velocities, erosion could be as much as 1.5 km, but not less than 1 km (Fig. 17B).

Second level: The layer is exposed at the seafloor to the southwest, and continues below the Cenozoic layer in the northeast, representing Upper Cretaceous strata. Velocities lie in the 3.0 to 3.45 km s^{-1} range. Erosion estimates are between 2.6 to 3.3 km in southern and central parts. The uncertainty to seismic velocity allows for an increased maximum of 200 m, but minimum estimates do not change much. The crossing Profile 6-03 (Breivik et al., 2017) was similarly analyzed (Fig. 17A). Erosion in the Ribban Basin is estimated to 3-3.5 km, while it appears less in the northern Vestfjorden Basin at about 2.4-2.7 km. The modeling was revisited to estimate velocity uncertainty on the sedimentary layers. For Ribban Basin, it is +0.05/-0.06 km s^{-1}, impacting minimum/maximum erosion estimates by ∼100 m. For Vestfjorden Basin, velocity cannot be lowered, but can be increased by 0.15 km s^{-1}, increasing maximum erosion estimate by 200 m.

Third level: There is a marked velocity contrast to the Lower Cretaceous layer below, despite the thinness of the overburden. Velocities range from 3.9 to 4.6 km s^{-1} on Profile 8-03. On the crossing Profile 6-03 they range from 4.1 to 4.9 km s^{-1} (Fig. 17). Uncertainties here are estimated to +0.05/-0.16 km s^{-1} for the Ribban Basin, and +0.73/-0.13 km s^{-1} for the Vestfjorden Basin. Velocities are higher than the best constrained part of the reference velocity curve, and quantification of erosion is tentative. West of the Utrøst High on Profile 6-03 the erosion could be 3-3.8 km. For Both the Havbåen Subbasin and the northern Vestfjorden Basin, erosion could be more than 4 km. Profile 8-03 indicates a minimum erosion of the Havbåen Subbasin of 3.4-3.9 km, but with a maximum up to 4.9 km. However, the present burial depth plus the erosion of level

2 above, suggests that erosion of this level cannot be determined north of ∼170 km in the model towards the Harstad Basin.

7. Discussion

Dating of the erosion levels from our data can only be approximate and the erosion estimates need to be interpreted in relation to what is known about regional tectonic events. On the other hand, our results may provide their own constraints on these, and the uncertainty of erosion estimates will be evaluated in relation to existing data. Also the large discrepancy between the older and the newer wide-angle seismic survey results on crustal thickness needs careful examination.

7.1. Erosion Method Evaluation

Our study is the first to publish results using seismic velocity or any quantitative method to estimate erosion on several stratigraphic levels on this part of the Norwegian shelf. However, compositional differences can affect the velocity-depth gradient as seen in the sonic log from well 7216/11-1S (Fig. 16). Both sands and carbonates may cause increased velocities compared to mudrocks at shallow depths, and composition appears to represent the greatest uncertainty with the method. The 1D velocity profiles extracted from Profile B-98 show a typical staircase function for this kind of modeling. Depth to the top of each velocity layer varies somewhat, and may be tied to lateral changes in composition, that the sonic log shows can be present. To smooth such factors, a distance range was therefore sampled for the curve fit. Other methods like thermal maturity, compaction, and apatite fission track analysis can in principle be used for quantitative erosion estimates. Studies from the Barents Sea show that different methods give similar trends between areas, but differ somewhat in absolute estimates (Baig et al., 2016; Henriksen et al., 2011; Ohm et al., 2008). Unfortunately, these methods require well measurements or core sampling, which are very limited in our study area.

The thermal maturity from a few shallow cores is only documented in unpublished reports. See Hansen et al. (2012) for a stratigraphic summary of these cores. The Norwegian Petroleum Directorate presents a summary of erosion estimates based on these in a report (NPD, 2010) (in Norwegian only). Four samples west of Røst to the south of our study area indicate 1000-1500 m of erosion. Another sample close to the coast in southern Vesterålen indicates 1700-1800 m of erosion. However, the best area for comparing our results with other estimates is on the northeastern part of Andøya, located inside of the northeastern end of our profile (Fig. 1), where maximum burial is 2000 m or more (NPD, 2010). Middle Jurassic sedimentary rocks exposed on land are coarse-grained and from non-marine deposition (Dalland, 1981). A marine transgression resulted in a mainly shaly Lower Cretaceous sequence of mostly Aptian age. Seismic velocity measurements within both the Jurassic and Cretaceous sections (Dalland, 1981) make it possible to compare with our method. Sandy Jurassic layers have velocities of 3.0-3.2 km s^{-1}, while the Lower Cretaceous shaly sequence has velocities of 2.4-2.5 km s^{-1}. Using the Cretaceous velocities with our red reference curve gives an erosion estimate of 1.6-1.8 km, while the blue curve gives 1.4 to 1.6 km. The red curve is most relevant to the shaly lithology. If we instead use the velocity of the Jurassic sandy layers, the estimates become 2.7 to 3.0 km (red curve) or 2.4 to 2.6 km (blue curve), where the blue curve is most relevant to the sandy lithology. Thus, our method gives results that are in reasonable agreement with the field studies from Andøya. Still, the comparisons suggest that there may be an uncertainty of $\pm$25% to erosion estimates. Even so, major erosion events should be detectable, and distinguishable from minor events.

7.2. Erosion Episodes

Seismic reflection data on the shelf show a thick Cretaceous package exposed at the seafloor, overlying a thin layer of Jurassic strata (e.g., Tsikalas et al., 2001; Hansen et al., 2012). In places there may be older deposits below, but these strata often appear to be resting directly on basement, suggesting removal of older sediments. A summary of the erosion episodes discussed here is found in Table 2. The first major episode occurred in Late Triassic – Early Jurassic times, where a field study from Andøya of a basement weathering profile, based on kaolinite blocking temperature for ^{40}Ar diffusion, indicates that 4-5 km was removed (Sturt et al., 1979). The southern part of our profile covers the western part of the Havbåen Subbasin (Fig. 10). Total depth is about 6 km, and the sedimentary rock velocities are the highest observed along profile. The deepest part consists of a layer 1.5-2 km thick with velocities of 5.0-5.4 km s^{-1}, about 1 km s^{-1} higher than the layer above, and too high for comparison to our Barents Sea reference. These may be upper

Paleozoic to early Mesozoic sedimentary strata denuded by the Late Triassic – Early Jurassic erosion event (e.g., Henstra et al., 2017). The interpretation of crossing reflection lines does not show much sedimentary thickness below the Base Cretaceous here (Hansen et al., 2012), suggesting that the amount of pre-Jurassic sedimentary strata may have been underestimated. The velocity of the lowest layer decreases somewhat to the northeast, where it could consist of younger rocks. Pre-Jurassic sediments could therefore be missing outside of the basin, possibly removed by this erosion event.

The tie to the crossing OBS Profile 6-03 (Breivik et al., 2017) is in the flank of the Utrøst Ridge (Fig. 17), where the sedimentary succession is thin. Here we find erosion level 3, which must be of an intra-Cretaceous age. On the crossing Profile 6-03, the top layer velocity is high next to the Utrøst Ridge and Lofoten, but falls to the middle parts of the basin indicating less erosion there, but still substantial. (Fig. 17A). Next to Lofoten the layer reaches the seafloor, where reflection seismic data show erosion down into Jurassic strata (Hansen et al., 2012). This is tied to fault development in Aptian to Albian times, where the Lofoten Ridge was uplifted and eroded (Løseth and Tveten, 1996). Structuring of the Utrøst Ridge also appears to be tied to this event. Erosion in the northern Vestfjorden Basin is similar on Profile 6-03 (Fig. 17A).

In the southwestern and central parts of Profile 8-03, erosion level 2 is at the seafloor (Fig. 17B). Off Vesterålen the top of this layer is buried under a layer mostly between 0.5 km and 1 km thick. Minimum and maximum burial depth estimates are 2.6 km and 3.5 km, respectively, greatest where the sedimentary layers are the thinnest (Fig. 17B). On Profile 6-03, erosion is similar in the Vestfjorden Basin on this level also (Fig. 17A). Presumably, this event is tied to Late Cretaceous to early Cenozoic erosion occurring around the time of continental breakup to the west (e.g., Færseth, 2012; Henstra et al., 2017). The top layer in the north appears to be of Cenozoic age, where young glacial erosion is the most likely mechanism to remove 1.0-1.5 km of sediment. A greater extent of erosion cannot be ruled out, since Cenozoic sediments are lacking to the southwest. However, the top layer velocities are falling in that direction, indicating that erosion could be restricted to the northeast of Profile 8-03.

The main results of this erosion investigation indicate a regional extent of the deep Late Triassic – Early Jurassic erosion recognized at Andøya. The mid-Cretaceous event has not been quantified before, and appears substantial for the ridges, but apparently affected the whole area (>4 km). The Utrøst Ridge/Jennegga High appears to have had its main development at this time, emphasizing an older origin than the Late Cretaceous – Paleogene uplift suggested by Henstra et al. (e.g. 2017), or the proposed Neogene uplift (Færseth, 2012), which is not identified in the velocity structure of the sedimentary strata over the high. The Late Cretaceous – Early Eocene erosion event that was recognized in the shallow cores, was in the summary by NPD (2010) restricted to the vicinity of the core locations and near offshore areas, and to the Vestfjorden Basin. The erosion analysis indicates that this is a more regional event, covering the offshore areas all the way to the shelf break. The analysis also indicates that it could be somewhat greater (2.5-3.4 km) than suggested by the single near-shore core off Vesterålen (1.7-1.8 km) nearest to our profile. It cannot be ruled out that some of this erosion is tied to Quaternary glaciations, though there is not much sediment transport down the continental slope adjacent to the shelf. There is a small fan outbuilding north of Bleiksdjupet, as well as the canyon itself at the northern end of Profile 8-03, correlating with the area where 1-1.5 km of late erosion is indicated.

The shelf area west of Lofoten and Vesterålen is dominated by the shallow basement of the Utrøst Ridge/Jennegga High, and the Ribban Basin is only a narrow depression. The mid-Cretaceous and Late Cretaceous to early Cenozoic erosion implies that burial of potential source rocks (e.g. Late Jurassic) may have been 2-3 km deeper before these events than they are presently, so that maximum burial and maturation would be in the Cretaceous. Also, the erosion could breach older reservoirs, and unloading causes expansion of gas in reservoirs, which drives out oil and gas, as seen in the Barents Sea (e.g., Ohm et al., 2008). The most prospective area there is in the Hammerfest Basin, where glacial erosion is moderate ($\sim$0.8-1.5 km) (Baig et al., 2016), and in basin flanks where gas and oil can migrate to a new reservoir higher in the stratigraphy during erosion (Ohm et al., 2008). Deeper erosion and a thin sedimentary cover makes this a less likely mechanism to preserve older reservoirs up to present on the Lofoten/Vesterålen shelf. Conditions change northeastwards off Vesterålen, where the sedimentary basin becomes deeper and erosion less towards the Harstad Basin. However, our data do not constrain this transitional area well.

7.3. *Continental Crustal Structure*

It is uncommon that the results of a newer OBS survey differ so greatly from the results of older, nearby studies as they do here. Crustal thickness of both Profile 6-03 (Breivik et al., 2017) and Profile 8-03 presented here is commonly 8 km to 16 km greater than seen in the older studies. When it comes to the difference between the NW-SE oriented Profiles 6-03 and 1-88 (Mjelde and Sellevoll, 1993), they are spaced so far apart ($\sim$100 km) that the differences could be real. On the other hand, Profile 6-03 crosses both Profile 8-03 and the old Sellevoll (1983) profile, and at the tie to the latter the Moho depth is $\sim$35 km, instead of their $\sim$25-26 km, which is far beyond the usual uncertainty of such studies of $\pm$1 km to $\pm$1.5 km (e.g., Breivik et al., 2005).

In refraction seismic, a secure Moho identification can be obtained from a combination of Moho reflections (P_MP) and upper mantle refractions (P_n). P_MP phases are characterized by high amplitude due to the large acoustic impedance contrast across the Moho boundary. However, high-amplitude reflections commonly also originate from the lower crust. When the reflection level can be tied to P_n phases a robust Moho identification can be made. The old Sellevoll (1983) study suggests that both P_n and P_MP phases can be identified in their data. However, seismic signals were recorded with land stations only, which resulted in strongly crooked line geometry. Furthermore, only one shot at each end of the profile were undertaken, resulting in little or no overlap where the deepest reflections and refractions occur, reducing structural control. Moho identification is not secure if control on layer dip is lacking.

At Profile 8-03, there are a number of P_MP phases, and two P_n phases (Figs. 4 and 5). The clearest P_MP phase is seen on OBS 88, and is a first arrival at offsets of between about 140 km to 150 km. On OBS 89, it is less clear but is seen as a first arrival at offsets of 160 to 170 km. The data quality of other stations is variable, and not all stations recorded far-offset arrivals. Given the $\sim$150 km length of the old Sellevoll (1983) profile in an area where the crust appears to be slightly thicker than at our profile, it is unlikely that this profile could record P_n phases, and that these were misidentified in the study. Both Profiles 8-03 and 6-03 have lower-crustal reflections of high amplitude, thus the reflections attributed to Moho on the old profile could originate from such reflective zones instead.

The greatest Moho depth of $\sim$36 km is recorded by Profile 6-03 (Breivik et al., 2017). If we only look at the shelf area and include the farthest land station, the offsets are up to ∼175 km. No secure Moho identification was obtained within this range. If we compare to the old Profile 1-88 (Mjelde and Sellevoll, 1993), it is similarly 175 km long lying on the shelf (Fig 1). There is no tie to that old profile, so it cannot be compared to newer results, but it could be treated with some caution in the light of the newer survey. As an example, a recent 3-D lithospheric density model of the region used constraints of different vintage (Maystrenko et al., 2017). The thick crust from Profile 6-03 was used in the northern part, and the thin crust of Profile 1-88 in the south. An enigmatic low-density mantle had to be introduced underneath the southern part of Lofoten in order to fit the regional gravity field. With a thicker crust, the need for such an anomalous mantle would be reduced or eliminated, and could potentially be an artifact.

The Moho depth does not reflect the highs and basins on top, and there may be a number of reasons for this. First of all, the basins are not very deep on the shelf, and crustal extension must have been minor. Extension may not have been pure shear, but distributed in the lower crust. Also the basin fill has high density, which could reduce Moho topography underneath through isostatic adjustment. Finally, pre-existing structure may have been smoothed by the Early Eocene extension tied to the continental breakup, apparently affecting the lower crust of the outer shelf to some degree (Breivik et al., 2017). However, the modeling result show that the crust of the shelf area is not strongly affected by the continental breakup.

Profile 8-03 shows a fairly uniform upper crystalline crustal structure of the shelf area, where velocities indicate a predominantly felsic to intermediate composition. The crustal structure is generally much simpler than that obtained from the crossing Profile 6-03 (Breivik et al., 2017). The latter crosses a number of different domains on the shelf, from the massive granite batholith of the Trans-Scandinavian Igneous Belt (TIB) underneath the mainland and eastern parts of the Vestfjorden Basin, to the increased seismic velocities of the Utrøst Ridge, indicating a change to a more intermediate composition. In the outer margin area northwest of our profile, the continental crystalline crust is extremely extended and has low velocities, indicating a felsic composition, but with a high-velocity lower-crustal body (LCB) underneath. The velocity of this body is 6.9-7.1 km s^{-1}, which is comparable to what is seen in the lower crust of Profile 8-03 (∼6.85-7.0 km s^{-1}). The composition of both these layers are therefore expected to be mafic, though the origin must be different. The LCB at the margin is completely continuous with the lower oceanic crust both in velocity and with Moho depth, which is typical for magma-rich continental margins. It is therefore interpreted as a massive intrusive complex emplaced during continental breakup. However, it tapers out ∼50 km from the continent-ocean transition zone, and does not reach the shelf area. It is also considerably smaller than the LCB seen at the Vøring Plateau (Mjelde et al., 2009).

On Profile 8-03, the lower crust is 10-14 km thick. It is not clear how this lower crustal layer continues towards the southeast under Lofoten/Vesterålen. However, it is thickest off the northern parts of Vesterålen, where the gravity field rises to the islands (Fig. 14), suggesting that it most likely increases in size to the southeast there. On Profile 6-03, it was terminated before it reached Lofoten, but this was poorly constrained. Nevertheless, it constitutes a substantial part of the crystalline crust of the outer shelf area. The last major crust-building episode of the area was tied to a Proterozoic subduction zone, which was also responsible for generating the TIB (e.g., Gradmann and Ebbing, 2015). Close to half of the exposed rocks in Lofoten/Vesterålen, ranging from gabbro to charnockite, were emplaced between 1700 and 1800 Ma (Griffin et al., 1978). It is therefore likely that much of the crust of the shelf dates back to this event, though an older component may be present in part.

8. Summary and Conclusions

Here we present a crustal velocity model of the continental shelf west of the islands of Lofoten/Vesterålen, based on the analysis of data from nine ocean bottom seismometers/hydrophones, part of a larger survey performed in 2003. Profile 8-03 covers the northern Ribban Basin (Havbåen Subbasin) northwest of Lofoten, the northern Utrøst Ridge (Jennegga High), and the flank of the Harstad Basin off Vesterålen. The sedimentary strata on the shelf mainly consists of Cretaceous layers, with some Cenozoic deposits on top in the northeast. The Havbåen Subbasin is up to 6 km deep at the profile, where the deepest layer is 1.5-2 km thick and may consist of upper Paleozoic and/or lower Mesozoic strata. Central parts of the profile over the Jennegga High have sedimentary layers 2-3 km thick. Off Vesterålen in the north, thickness increases to 3-5 km, but further increase in the flank of the Harstad Basin at the northeastern end of the profile is poorly constrained by the data.

Sedimentary velocities are very high compared to the present burial depth, indicating four erosional episodes along the profile. The Late Triassic - Early Jurassic episode is known to be extensive, but was not quantified here. The other episodes were tentatively quantified by comparing the velocity-depth curves to a reference constructed from OBS data and a well log in the southwestern Barents Sea. A mid-Cretaceous event was estimated to have removed $>$4 km of sediments from the Havbåen Subbasin. Erosion was deeper but not quantified over the Jennegga High in the central parts of the model, but may be absent in the flank of the Harstad Basin. A continental breakup-related Late Cretaceous to early Cenozoic erosional episode has given high velocities exposed at the seafloor in southwestern parts, indicating 2.6-3.5 km of denudation. Off Vesterålen, erosion of the Cenozoic layer is estimated to 1.0-1.5 km, likely tied to the glaciations in the latest Cenozoic. This erosional history most likely destroyed any petroleum system that may have existed in the past.

Most of the upper crystalline crust has velocities of 6.0-6.3 km s^{-1}. Velocity increases downward in the upper half of the crust to just above 6.6 km s^{-1}, while the lower crust has velocities of 6.85-7.0 km s^{-1}. The top of the lower crust gives high-amplitude reflections, also seen from within its interior in the south. Moho depth is well constrained to $\sim$31 km depth in central parts from Moho reflections and refractions from the uppermost mantle, and by the tie to the crossing Profile 6-03 (Breivik et al., 2017). Gravity modeling constrained the Moho depth to continue on this level southwest of the tie. Crustal thickness of the area obtained from the OBS 2003 survey (this study, and Breivik et al. (2017)) is significantly higher than that found by Sellevoll (1983). It appears that the old survey was too short to constrain true crustal thickness here.

References

Baig, I., Faleide, J.I., Jahren, J., Mondol, N.H., 2016. Cenozoic exhumation on the southwestern Barents Shelf: Estimates and uncertainties constrained from compaction and thermal maturity analyses. Mar. Petrol. Geol. 73, 105–130. doi:10.1016/j.marpetgeo.2016.02.024.

Barton, P.J., 1986. The relationship between seismic velocity and density in the continental crust – A useful constraint? Geophys. J. R. Astron. Soc. 87, 195–208.

Bergh, S.G., Eig, K., Kløvjan, O.S., Henningsen, T., Olesen, O., Hansen, J.A., 2007. The Lofoten-Vesterålen continental margin: a multiphase Mesozoic-Palaeogene rifted shelf as shown by offshore-onshore brittle fault-fracture analysis. Norw. J. Geol. 87, 29–58.

Bezada, M.J., Zelt, C.A., 2011. Gravity inversion using seismically derived crustal density models and genetic algorithms: an application to the Caribbean–South American Plate boundary. Geophys. J. Int. 185, 577–592. doi:10.1111/j.1365-246X.2011.04965.x.

Breivik, A.J., Faleide, J.I., Gudlaugsson, S.T., 1998. Southwestern Barents Sea margin: late Mesozoic sedimentary basins and crustal extension. Tectonophysics 293, 21–44.

Breivik, A.J., Faleide, J.I., Mjelde, R., Flueh, R., Murai, Y., 2017. A new tectono-magmatic model for the Lofoten/Vesterålen Margin at the outer limit of the Iceland Plume influence. Tectonophysics 718, 25–44. doi:10.1016/j.tecto.2017.07.002.

Breivik, A.J., Mjelde, R., Grogan, P., Shimamura, H., Murai, Y., Nishimura, Y., 2005. Caledonide development offshore-onshore Svalbard based on Ocean Bottom Seismometer, conventional seismic, and potential field data. Tectonophysics 401, 79–117. doi:10.1016/j.tecto.2005.03.009.

Breivik, A.J., Mjelde, R., Grogan, P., Shimamura, H., Murai, Y., Nishimura, Y., Kuwano, A., 2002. A possible Caledonide arm through the Barents Sea imaged by OBS data. Tectonophysics 355, 67–97.

Chroston, P.N., Brooks, S.G., 1989. Lower crustal seismic velocities from Lofoten-Vesterålen, north Norway. Tectonophysics 157, 251–269.

Dalland, A., 1981. Mesozoic sedimentary succession at Andøy, Northern Norway, and relation to structural development of the north Atlantic area. Mem. Can. Soc. Petrol. Geol. 7, 563–584.

Færseth, R.B., 2012. Structural development of the continental shelf offshore Lofoten–Vesterålen, northern Norway. Norw. J. Geol. 92, 19–40.

Faleide, J.I., Tsikalas, F., Breivik, A.J., Mjelde, R., Ritzmann, O., Engen, Ø., Wilson, J., Eldholm, E., 2008. Structure and evolution of the continental margin off Norway and the Barents Sea. Episodes 31, 82–91.

Gradmann, S., Ebbing, J., 2015. Large-scale gravity anomaly in northern Norway: tectonic implications of shallow or deep source depth and a possible conjugate in northeast Greenland. Geophys. J. Int. 203, 2070–2088. doi:10.1093/gji/ggv426.

Griffin, W.L., Taylor, P.N., Hakkinen, J.W., Heier, K.S., Iden, I.K., Krogh, E.J., Malm, O., Olsen, K.I., Ormaasen, D.E., Tveten, E., 1978. Archaean and Proterozoic crustal evolution in Lofoten–Vesterålen, N Norway. J. Geol. Soc. 135, 629–647. doi:10.1144/gsjgs.135.6.0629.

Hansen, J.A., Bergh, S.G., Henningsen, T., 2012. Mesozoic rifting and basin evolution on the Lofoten and Vesterålen Margin, North-Norway; time constraints and regional implications. Norw. J. Geol. 91, 203–228.

Heasler, H.P., Kharitonova, N.A., 1996. Analysis of sonic well logs applied to erosion estimates in the Bighorn Basin, Wyoming. AAPG Bull. 80, 630–646.

Henriksen, E., Bjørnseth, H.M., Hals, T.K., Heide, T., Kiryukhina, T., Kløvjan, O.S., Larssen, G.B., Ryseth, A.E., Rønning, K., Sollid, K., Stoupakova, A., 2011. Uplift and erosion of the greater Barents Sea: impact on prospectivity and petroleum systems, in: Spencer, A.M., Embry, A.F., Gautier, D.L., Stoupakova, A.V., Sørensen, K. (Eds.), Arctic Petroleum Geology. Geol. Soc., London. volume 35 of *Mem.*, pp. 271–281. doi:10.1144/M35.17.

Henstra, G.A., Gawthorpe, R.L., Helland-Hansen, W., Ravnås, R., Rotevatn, A., 2017. Depositional systems in multiphase rifts: seismic case study from the Lofoten margin, Norway. Bas. Res. 29, 447–469. doi:10.1111/bre.12183.

Jakobsson, M., Mayer, L.A., Coakley, B., Dowdeswell, J.A., Forbes, S., Fridman, B., Hodnesdal, H., Noormets, R., Pedersen, R., Rebesco, M., Schenke, H.W., Zarayskaya, Y., Accettella, A.D., Armstrong, A., Anderson, R.M., Bienhoff, P., Camerlenghi, A., Church, I., Edwards, M., Gardner, J.V., Hall, J.K., Hell, B., Hestvik, O.B., Kristoffersen, Y., Marcussen, C., Mohammad, R., Mosher, D., Nghiem, S.V., Pedrosa, M.T., Travaglini, P.G., Weatherall, P., 2012. International Bathymetric Chart of the Arctic Ocean (IBCAO) Version 3.0. Geophys. Res. Lett. 39. doi:10.1029/2012GL052219.

Løseth, H., Tveten, E., 1996. Post-Caledonian structural evolution of the Lofoten and Vesterålen offshore and onshore areas. Norsk Geol. Tidsskr. 76, 215–230.

Maystrenko, Y.P., Olesen, O., Gernigon, L., Gradmann, S., 2017. Deep structure of the Lofoten-Vesterålen segment of the Mid-Norwegian continental margin and adjacent areas derived from 3-D density modeling. J. Geophys. Res. Solid Earth 122, 1402–1433. doi:10.1002/2016JB013443.

Mjelde, R., Breivik, A.J., Elstad, H., Ryseth, A.E., Skilbrei, J.R., Opsal, J.G., Shimamura, H., Murai, Y., Nishimura, Y., 2002. Geological development of the Sørvestsnaget Basin, SW Barents Sea, from ocean bottom seismic, surface seismic, and potential field data. Norw. J. Geol. 82, 183–202.

Mjelde, R., Faleide, J.I., Breivik, A.J., Raum, T., 2009. Lower crustal composition and crustal lineaments on the Vøring Margin, NE Atlantic: A review. Tectonophysics 427, 183–193. doi:10.1016/j.tecto.2008.04.018.

Mjelde, R., Kodaira, S., Shimamura, H., Kanazawa, T., Shiobara, H., Berg, E.W., Riise, O., 1997. Crustal structure of the central part of the Vøring Basin, mid-Norway margin, from ocean bottom seismographs. Tectonophysics 277, 235–257.

Mjelde, R., Raum, T., Breivik, A., Shimamura, H., Murai, Y., Takanami, T., Faleide, J.I., 2005. Crustal structure of the Vøring Margin, NE Atlantic: a review of geological implications based on recent OBS data, in: Doré, A.G., Vining, B.A. (Eds.), Petroleum Geology: North-West Europe and Global Perspectives - Proceedings of the 6th Petroleum Geology Conference, Geol. Soc., London. pp. 803–814.

Mjelde, R., Sellevoll, M.A., 1993. Possible shallow crustal anisotropy off Lofoten, Norway, inferred from three-component ocean-bottom seismographs. Geophys. J. Int. 115, 159–167.

Mjelde, R., Sellevoll, M.A., Shimamura, H., Iwasaki, T., Kanazawa, T., 1992. A crustal study off Lofoten, N. Norway

by use of 3-C ocean bottom seismographs. Tectonophysics 212, 269–288.
Mjelde, R., Sellevoll, M.A., Shimamura, H., Iwasaki, T., Kanazawa, T., 1993. Crustal structure under Lofoten, N. Norway, from vertical incidence and wide-angle data. Geophys. J. Int. 114, 116–126.
Nafe, J.E., Drake, C.L., 1957. Variation with depth in shallow and deep water marine sediments of porosity, density and the velocities of compressional and shear waves. Geophysics 22, 523–552.
NPD, 2010. Geofaglig vurdering av petroleumsressursene i havområdene utenfor Lofoten, Vesterålen og Senja. https://www.npd.no/globalassets/1-npd/publikasjoner/rapporter/2010---rapport---geofaglig-vurdering-av-petroleumsressursene-i-havomradene-utenfor-lofoten-vesteralen-og-senja.pdf. Norwegian Petroleum Directorate. Stavanger, Norway.
Ohm, S.E., Karlsen, D.A., Austin, T.J.F., 2008. Geochemically driven exploration models in uplifted areas: Examples from the Norwegian Barents Sea. AAPG Bull. 92, 1191–1223. doi:10.1306/06180808028.
Olesen, O., Brönner, M., Ebbing, J., Gellein, J., Gernigon, L., Koziel, J., Lauritsen, T., Myklebust, R., Pascal, C., Sand, M., Solheim, D., Usov, S., 2010. New aeromagnetic and gravity compilations from Norway and adjacent areas: methods and applications, in: Vining, B.A., Pickering, S.C. (Eds.), Petroleum Geology: From Mature Basins to New Frontiers – Proceedings of the 7th Petroleum Geology Conference, Geol. Soc., London. pp. 559–586. doi:10.1144/0070559.
Ormaasen, D.E., 1977. Petrology of the Hopen mangerite-charnockite intrusion, Lofoten, north Norway. Lithos 10, 291–310.
Osmundsen, P.T., Ebbing, J., 2008. Styles of extension offshore mid-Norway and implications for mechanisms of crustal thinning at passive margins. Tectonics 27, TC6016. doi:10.1029/2007TC002242.
Rise, L., Bøe, R., Riis, F., Bellec, V.K., Laberg, J.S., Eidvin, T., Elvenes, S., Thorsnes, T., 2013. The Lofoten-Vesterålen continental margin, North Norway: canyons and mass-movement activity. Mar. Petr. Geol. 45, 134–149. doi:10.1016/j.marpetgeo.2013.04.021.
Ryseth, A., Augustson, J.H., Charnock, M., Haugerud, O., Knutsen, S.M., Midbøe, P.S., Opsal, J.G., Sundsbø, G., 2003. Cenozoic stratigraphy and evolution of the Sørvestsnaget Basin, southwestern Barents Sea. Norw. J. Geol. 83, 107–130.
Schlinger, C.M., 1985. Magnetization of lower crust and interpretation of regional magnetic anomalies: example from Lofoten and Vesterålen, Norway. J. Geophys. Res. 90, 11484–11504.
Sellevoll, M.A., 1983. A study of the Earths crust in the island area of Lofoten-Vesterålen, northern Norway. Nor. Geol. Unders. Bull. 380, 235–243.
Sturt, B.A., Dalland, A., Mitchell, J.L., 1979. The age of the sub Mid-Jurassic tropical weathering profile of Andøya, northern Norway, and the implications for the late Palaeozoic palaeography in the North Atlantic region. Geol. Rund. 68, 523–542. doi:10.1007/BF01820805.
Talwani, M., Worzel, J.L., Landisman, M.G., 1959. Rapid gravity computations for two-dimensional bodies with

application to the Mendocino submarine fracture zone. J. Geophys. Res. 64, 49–59.

Tasrianto, R., Escalona, A., 2015. Rift architecture of the Lofoten-Vesterålen margin, offshore Norway. Mar. Petr. Geol. 64, 1–16. doi:10.1016/j.marpetgeo.2015.02.036.

Tsikalas, F., Faleide, J.I., Eldholm, O., 2001. Lateral variations in tectono-magmatic style along the Lofoten–Vesterålen volcanic margin off Norway. Mar. Petrol. Geol. 18, 807–832.

Wessel, P., Smith, W.H.F., 1991. Free software helps map and display data. Eos Trans. AGU 72, 441,445–446.

Wessel, P., Smith, W.H.F., Scharroo, R., Luis, J.F., Wobbe, F., 2013. Generic Mapping Tools: Improved version released. EOS Trans. AGU 94, 409–410.

Zelt, C.A., Smith, R.B., 1992. Seismic traveltime inversion for 2-D crustal velocity structure. Geophys. J. Int. 108, 16–34.

Acknowledgments

We thank H. Shimamura, O. Ritzmann, and A. Krabbenhöft for their invaluable participation in planning, executing, and initial processing of the OBS data, and C. Zelt for the forward/inversion seismic modeling software. The Research Council of Norway funded the wide-angle seismic survey under the European Science Foundation Euromargins program (CRP01). Additional funding was provided by the Large Scale Facility at GEOMAR, Germany, Project HPRI-CT-2001-00154. A.J. Breivik and J.I. Faleide acknowledge support from the Research Council of Norway through its Centres of Excellence funding scheme, project number 223272. We thank two anonymous reviewers for the many helpful comments on how to improve the manuscript. The survey-specific data can be obtained by contacting authors A.J. Breivik or R. Mjelde. O. Olesen of the Geological Survey of Norway provided the gravity grid. High-resolution topography/bathymetry is freely available from the Norwegian Mapping Authority (www.kartverket.no). Declarations of interest: none.

Table 1: Seismic model fit statistics for the major refracted phases and the Moho reflection, and a summary of the listed phases. The phases P_{X1-4} indicate sedimentary layers, numbered from the top. Similarly for the basement refracted phases P_{g1-3}, 1-3 indicate upper, middle, and lower crustal layers, respectively. Suffix (h) indicates that the phase is modeled as a head wave. The water layer arrivals and some reflections (140 pts.) are not tabulated.

Phase	**No. rays**	**RMS $\triangle$t (ms)**	χ^2
P_{X1}	26	0.041	0.704
P_{X2}	193	0.049	0.789
P_{X3}	149	0.057	0.589
P_{X4}	132	0.061	0.496
$P_{X4(h)}$	10	0.097	1.043
P_{g1}	191	0.062	0.358
$P_{g1(h)}$	497	0.093	0.832
P_{g2}	419	0.079	0.577
P_{g3}	146	0.108	1.136
P_n	16	0.058	0.160
P_MP	111	0.130	0.728
All phases	1890	0.082	0.688

Table 2: Summary of four erosion episodes recognized on the Lofoten/Vesterålen shelf. Level refers to erosion levels in Figure 17. The erosion estimate for the earliest episode is from Sturt et al. (1979) for Andøya.

Period/Epoch	Level	Erosion estimate	Affected area
Quaternary	1	1.0 to 1.5 km	Off northern Vesterålen
Late Cretaceous – Early Eocene?	2	2.6-3.5 km	Regional
Mid-Cretaceous	3	>3 km	Off Lofoten and southern Vesterålen, northern Vestfjorden Basin, greatest at the Utrøst Ridge and adjacent Lofoten Ridge
Late Triassic – Early Jurassic		4-5 km	Havbåen Subbasin, Andøya, regional?

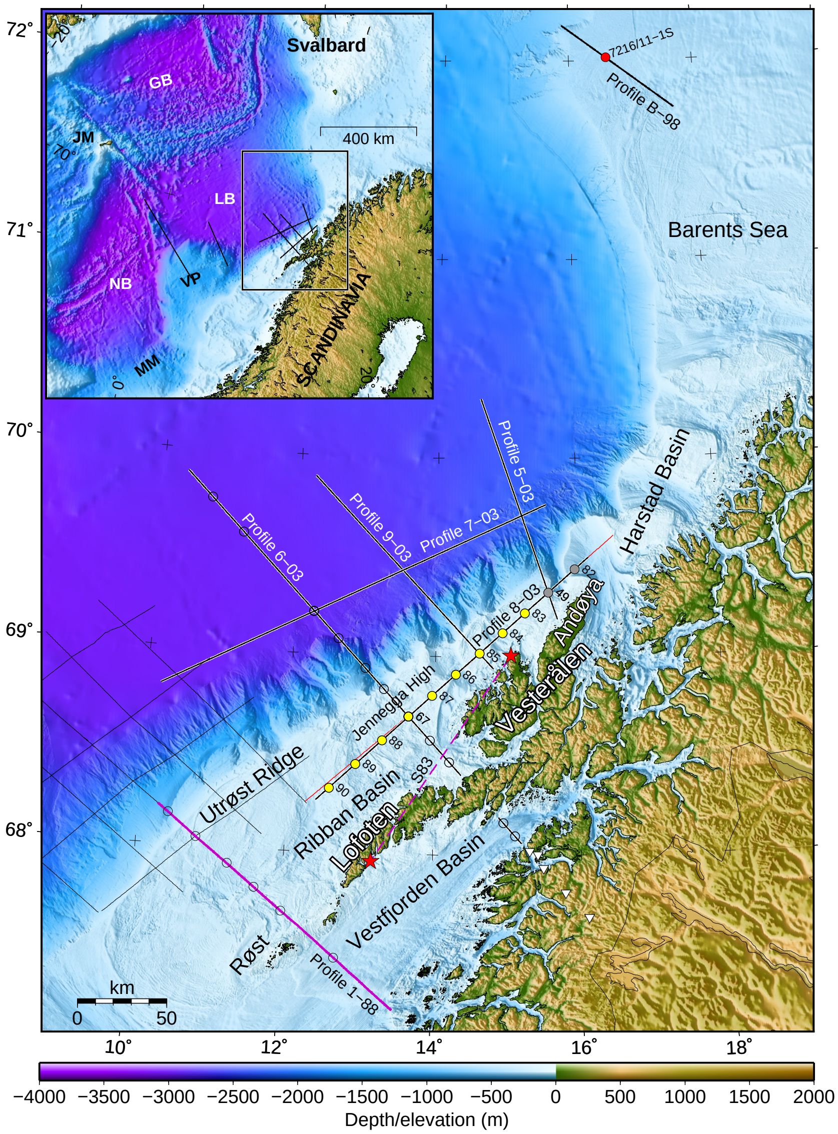

Figure 1: 200 m resolution topography and sidescan bathymetry downsampled from 50 m resolution data (©Kartverket). Deep ocean bathymetry is IBCAO v.3 (Jakobsson et al., 2012). Euromargins 2003 OBS lines are shown by bold black lines. OBS positions giving data on Profile 8-03 are shown with yellow-filled circles, while gray fill mark failed stations. Red line along the profile shows position of MCS line in Fig.2. Unfilled circles and white inverted triangles on Profile 6-03 show stations used to determine continental crustal structure by Breivik et al. (2017). The 1988 OBS survey is shown by thin lines. Profile 1-88 from Mjelde et al. (1993) is shown by a thick, purple line, where OBSs used are shown by open circles. The forward/reverse shot locations for the land-station profile (S83) from Sellevoll (1983) are shown by red stars, connected by a dashed purple line. Inset map: Frame shows study location. GB: Greenland Basin, JM: Jan Mayen, LB: Lofoten Basin, NB: Norway Basin, VP: Vøring Plateau.

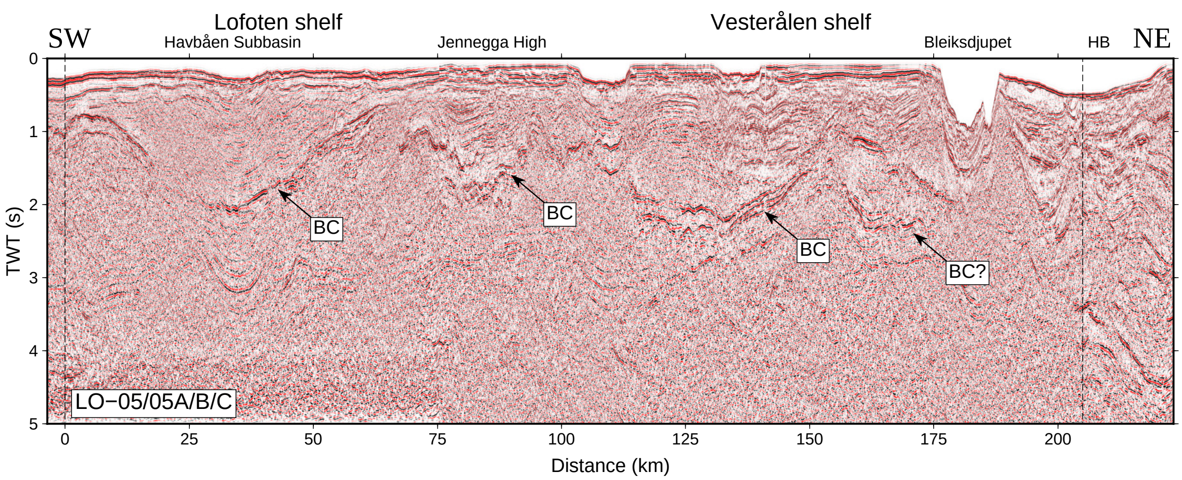

Figure 2: Multichannel reflection seismic line along OBS profile, merged from four individual sections shot in 1986; LO-05-86, LO-05-86A, LO-05-86B, and LO-05-86C. The overlap of the OBS profile is indicated by the dashed vertical lines, and the distance scale follows the OBS profile. The most prominent reflector is believed to represent the Base Cretaceous, marked BC on the section. HB: Harstad Basin.

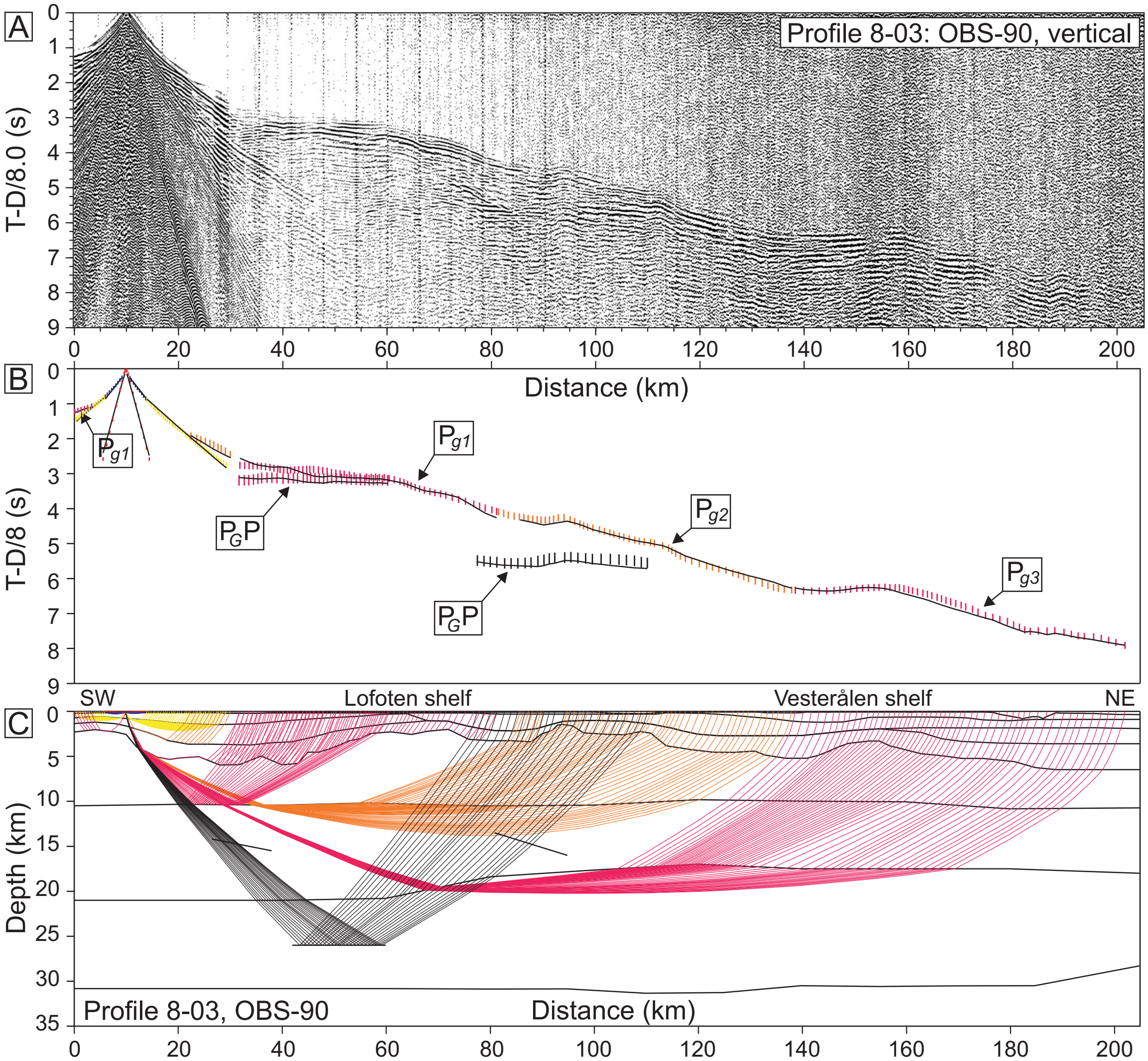

Figure 3: Data, interpretation, and ray tracing of OBS 90, Profile 8-03. A: OBS data, vertical component, offset-dependent scaling. B: Interpretation (vertical bars) and model prediction (solid lines). C: Ray tracing of the velocity model. Vertical exaggeration is 1.73.

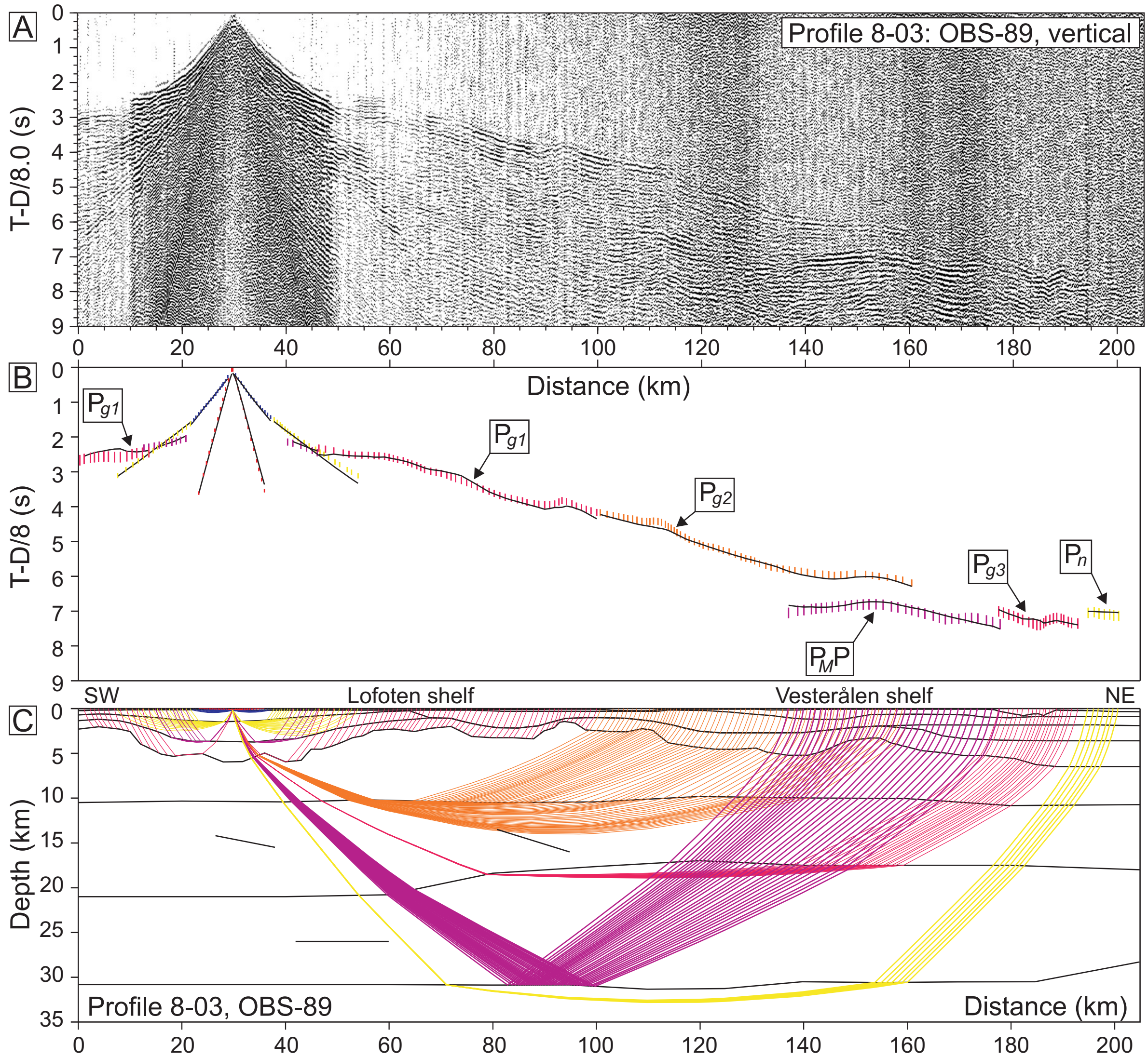

Figure 4: Data, interpretation, and ray tracing of OBS 89, vertical component, Profile 8-03. See Figure 3 for details.

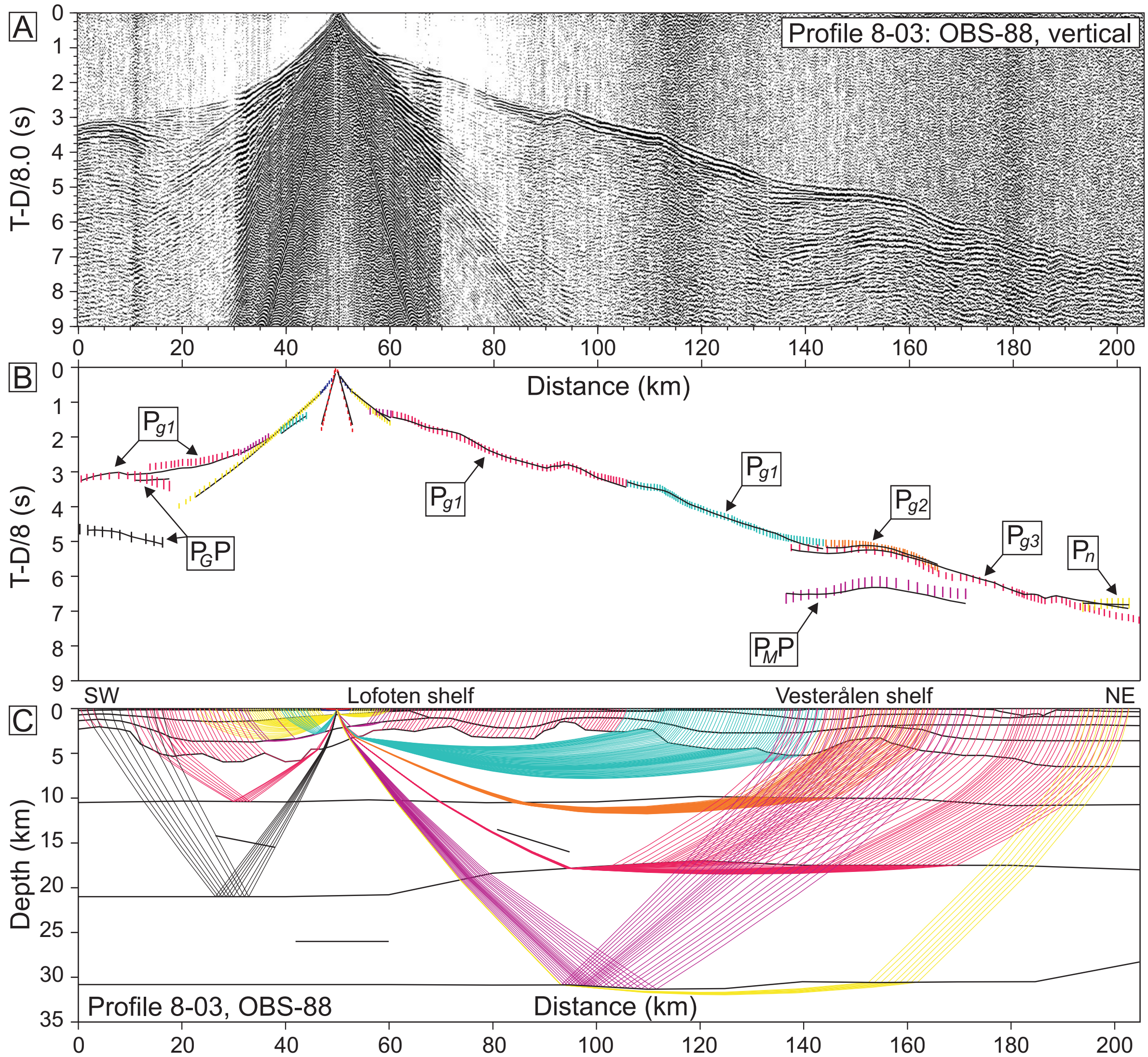

Figure 5: Data, interpretation, and ray tracing of OBS 88, vertical component, Profile 8-03. See Figure 3 for details.

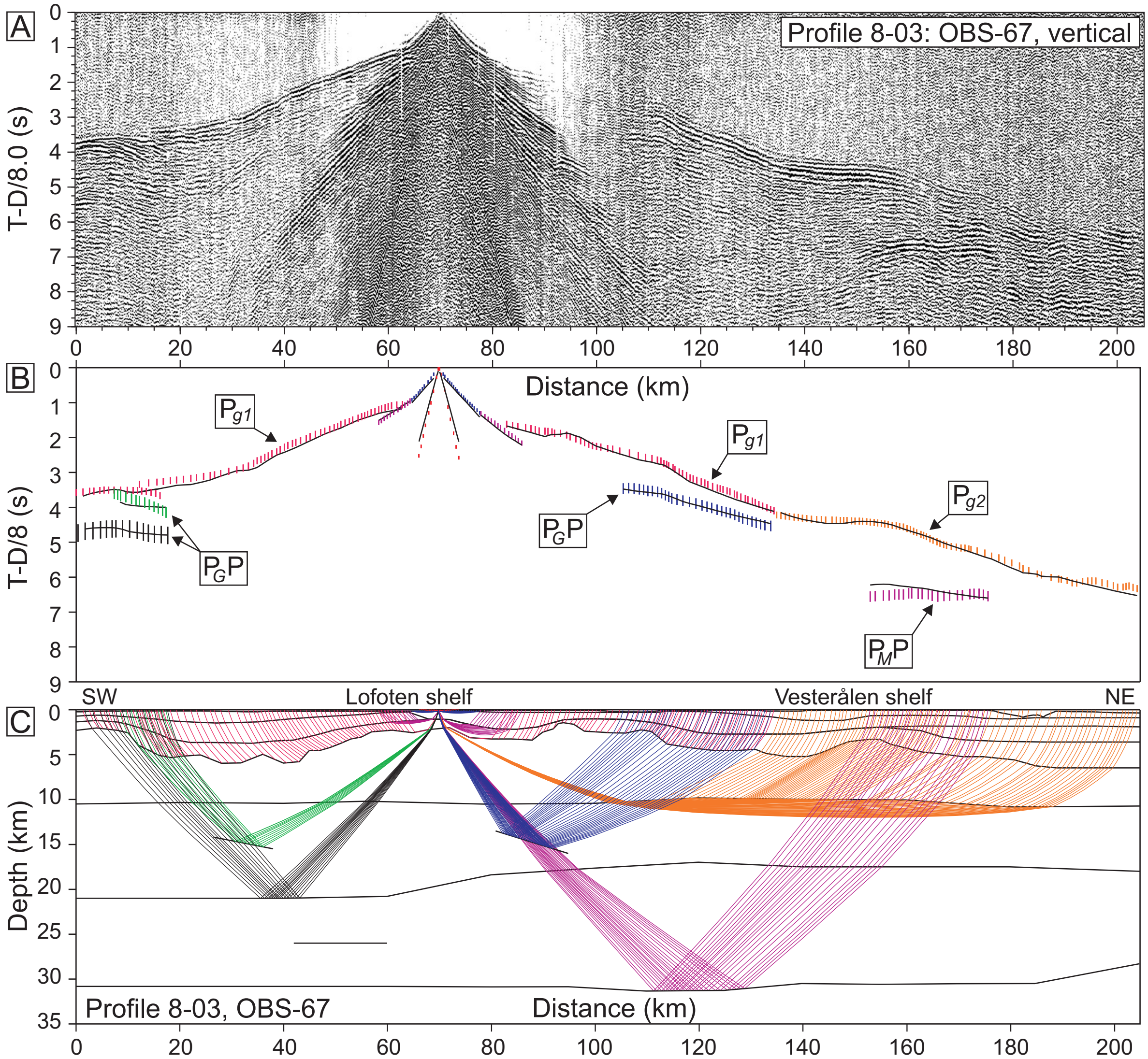

Figure 6: Data, interpretation, and ray tracing of OBS 67, vertical component, Profile 8-03. See Figure 3 for details.

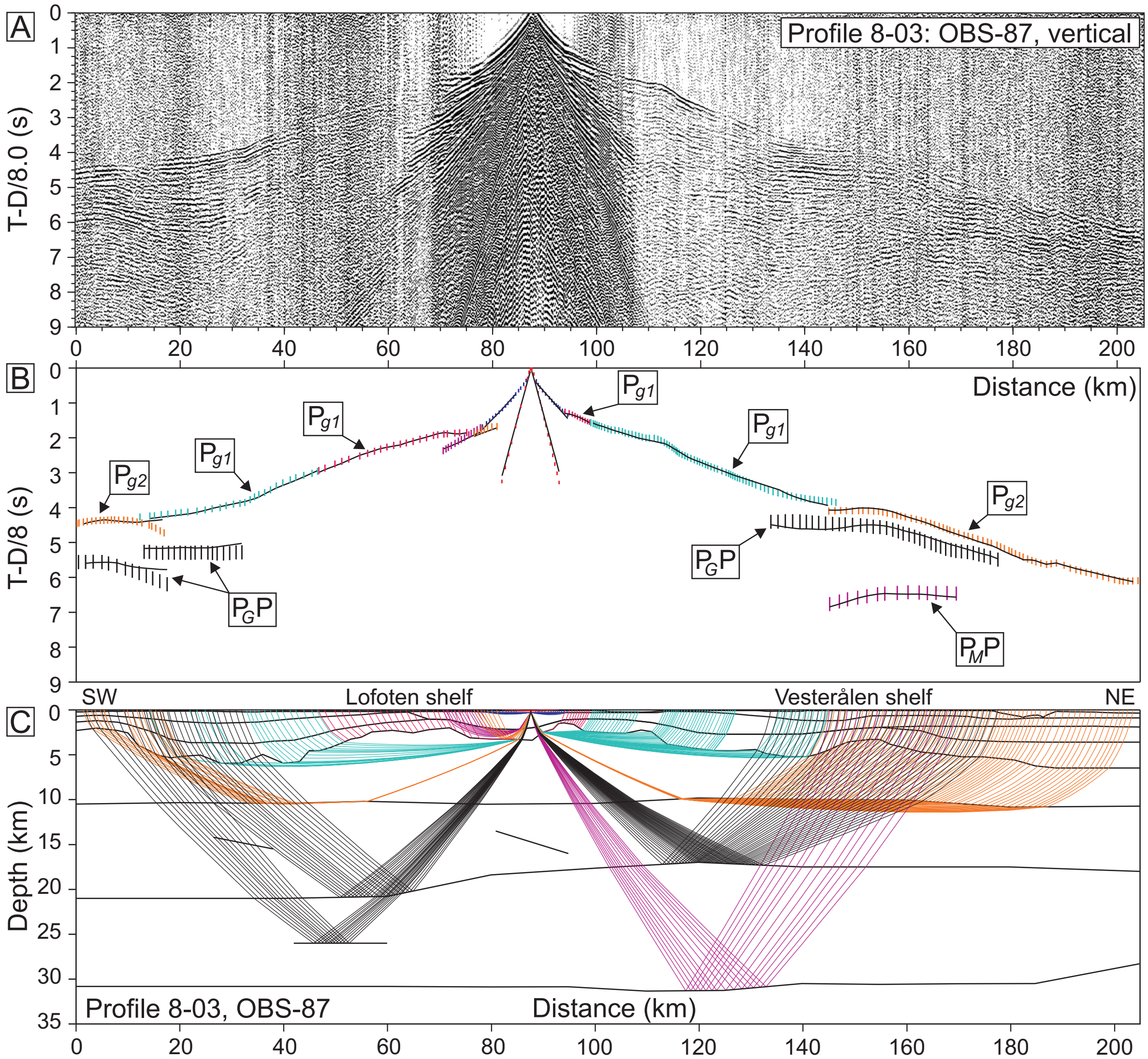

Figure 7: Data, interpretation, and ray tracing of OBS 87, vertical component, Profile 8-03. See Figure 3 for details.

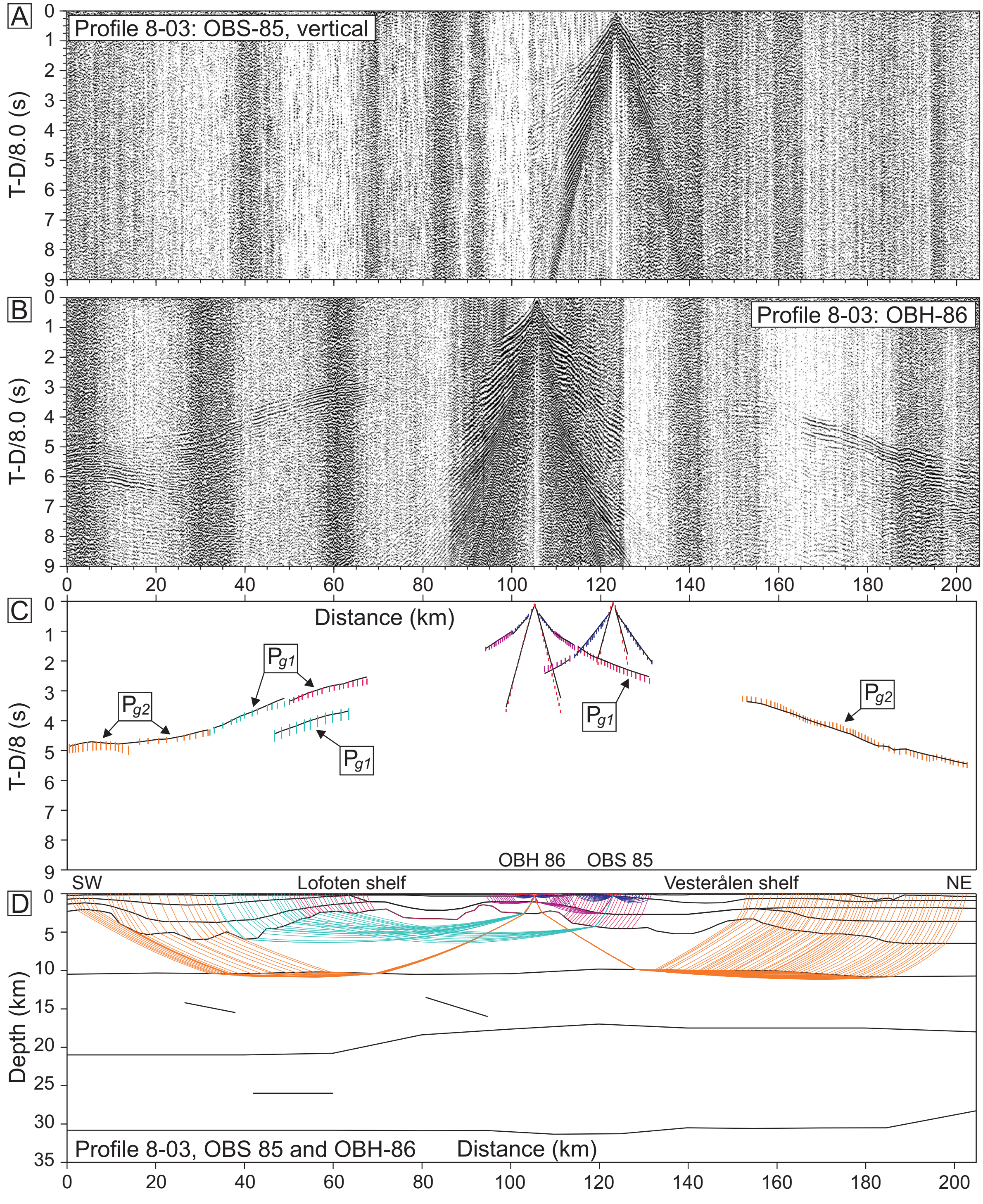

Figure 8: Data, interpretation, and ray tracing of A: OBS 85, vertical component, and B: OBH 86, Profile 8-03. C: Interpretation (vertical bars) and model prediction (solid lines) for both data sets. D: Ray tracing for both data sets of the velocity model. Vertical exaggeration is 1.73.

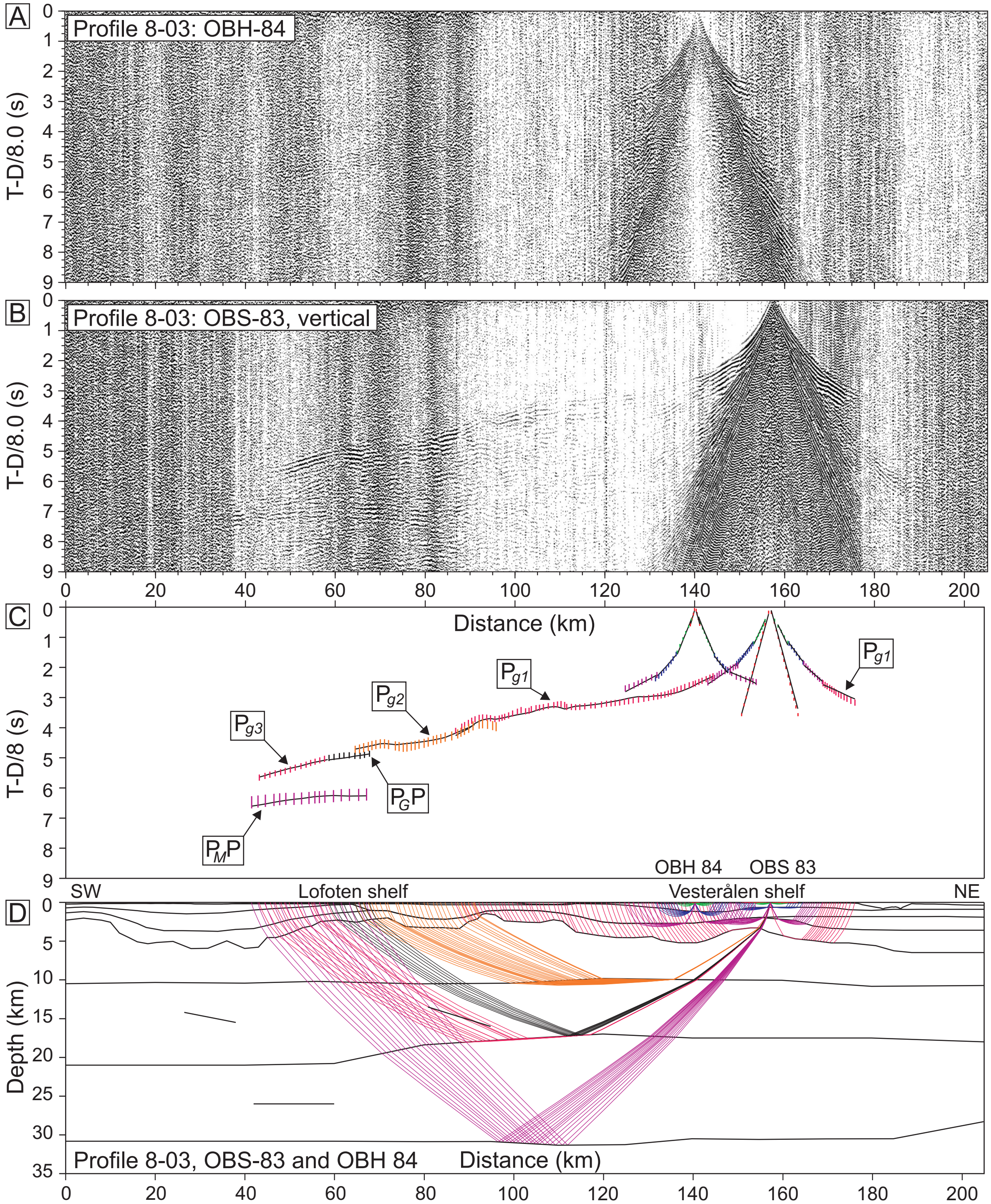

Figure 9: Data, interpretation, and ray tracing of A: OBH 84, and B: OBS 83, vertical component, Profile 8-03. See Figure 8 for details.

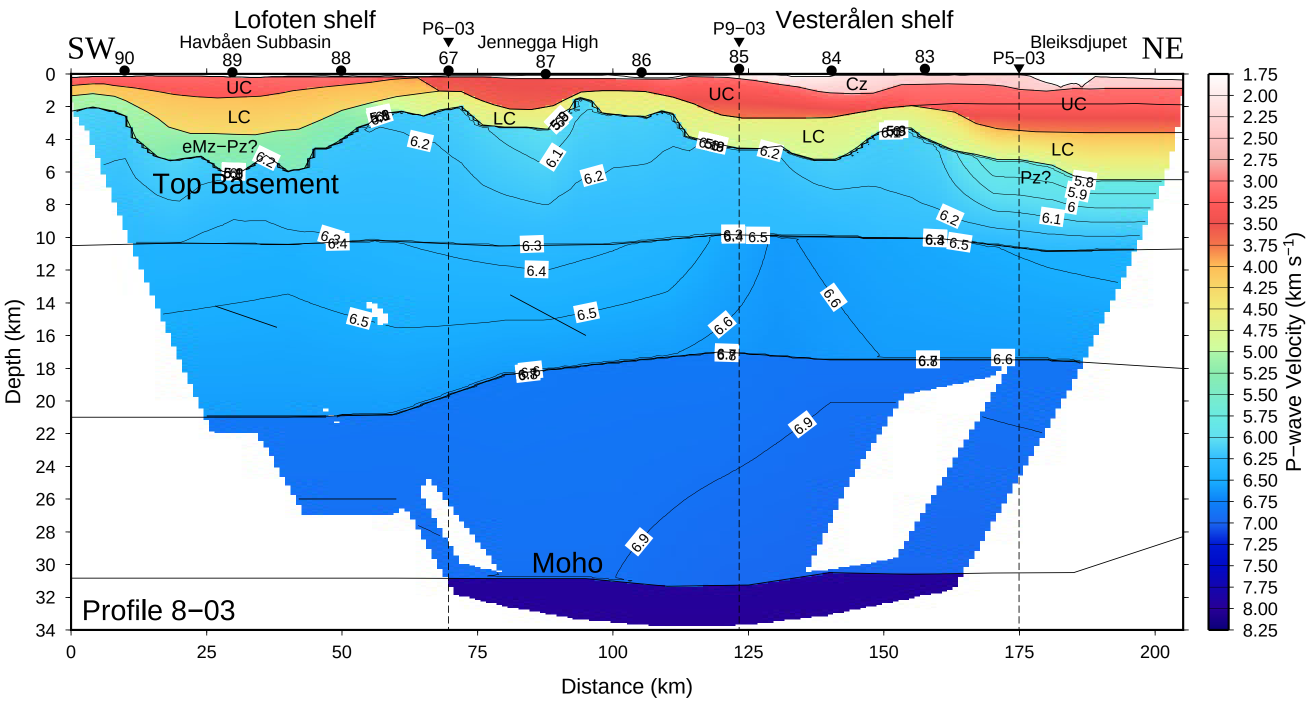

Figure 10: Gridded crustal velocity model of Profile 8-03, showing ray coverage. The OBS/H locations are numbered on the seafloor. Tentative geological ages for the sedimentary layers are indicated; Cz: Cenozoic, UC: Upper Cretaceous, LC: Lower Cretaceous, eMz-Pz: early Mesozoic-Paleozoic. Pz: Paleozoic. The ties to Profiles 6-03 and 9-03 are indicated by the inverted triangles and vertical dashed lines. Basement velocities are gridded and annotated. Vertical exaggeration is 1:3.

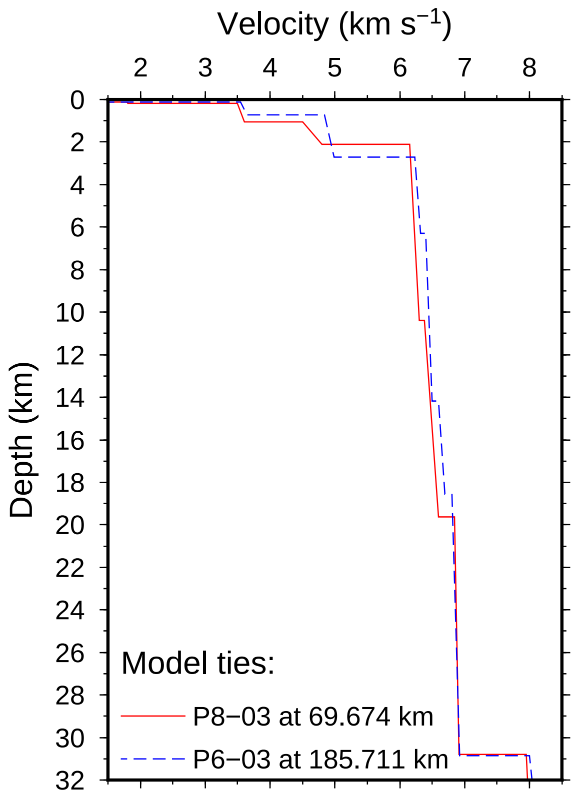

Figure 11: Sampled 1D velocity profiles from the tie between OBS models of Profile 8-03, and Profile 6-03 from Breivik et al. (2017).

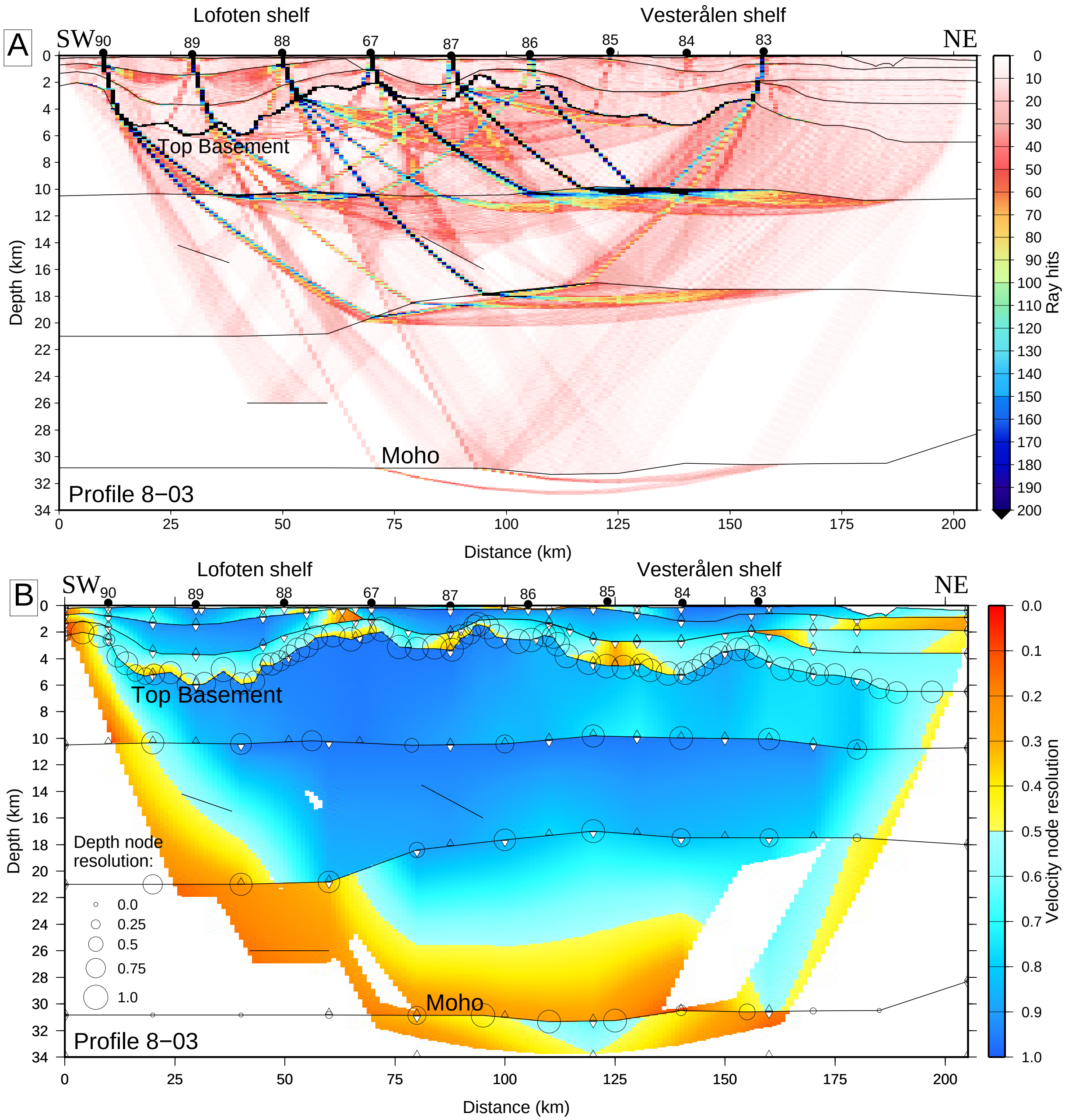

Figure 12: Ray coverage and resolution values. A: Gridded ray coverage of the Profile 8-03 velocity model. The binning is 2.5 km horizontally and 0.25 km with depth. B: Gridded resolution parameters of the P-wave velocity nodes obtained from inversion shown by color scale. Velocity node positions at the top of layers are shown by white-filled inverted triangles, while bottom layer node positions are shown by open triangles. Depth node resolution from top of the crystalline crust to the Moho is shown by the size of the circles enclosing them. Vertical exaggeration is 1:3 for both panels.

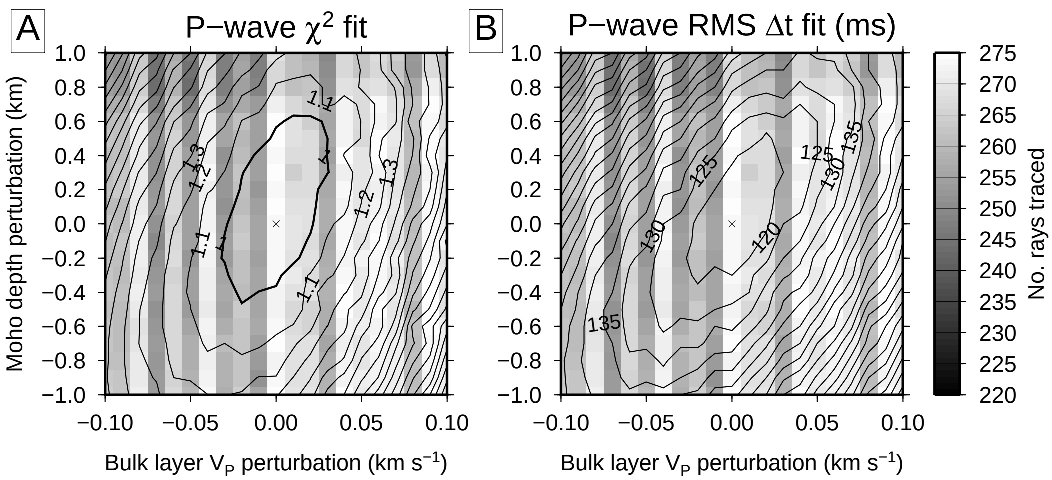

Figure 13: Model sensitivity to changes in Moho depth versus variations in lower crustal P-wave velocities. Deeper gray shading indicates increasing loss of rays. A: χ^2 fit based on $P_M P$, P_{g3}, and P_n phases. B: Corresponding RMS Δt misfit in milliseconds (ms).

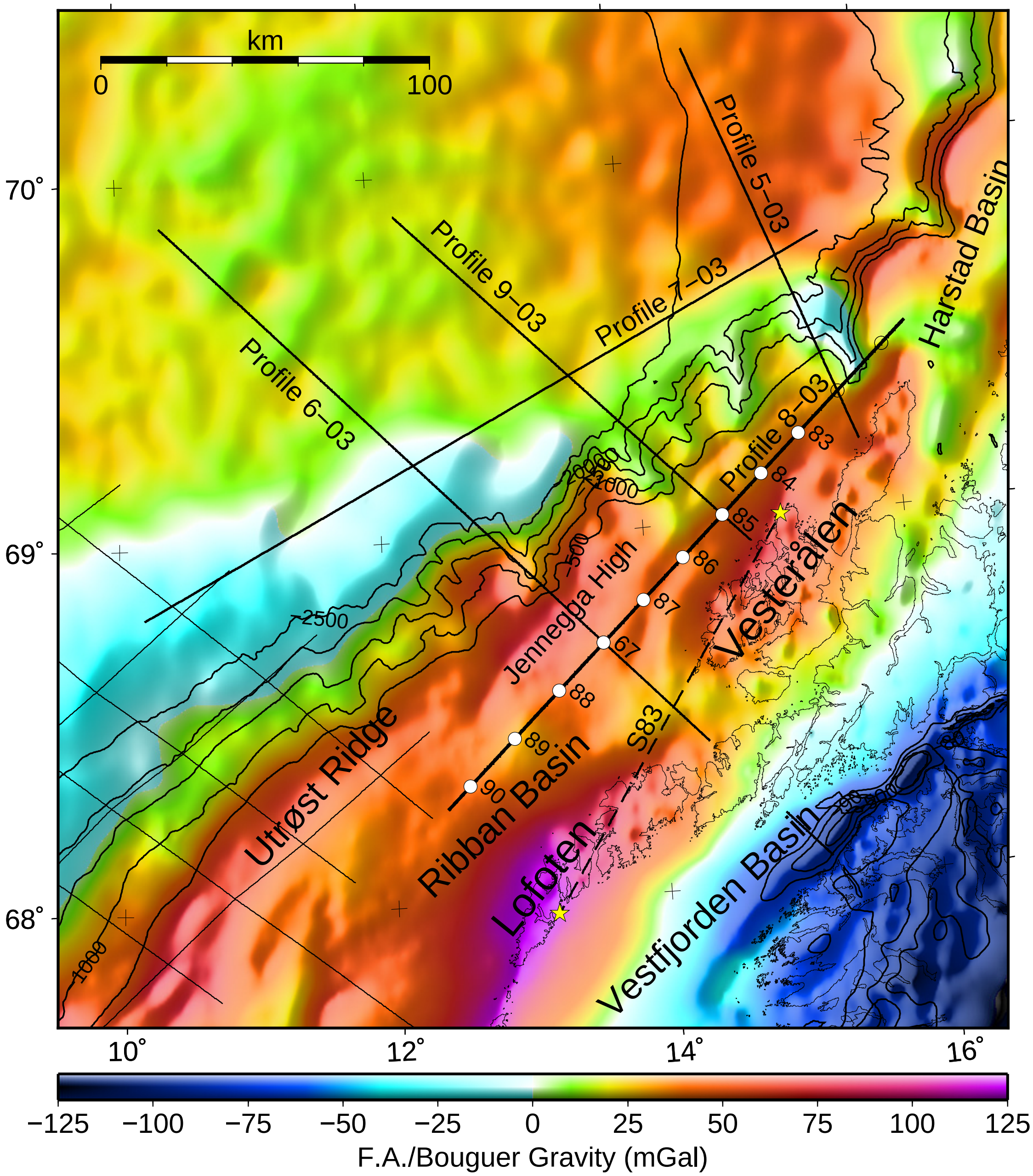

Figure 14: Marine free-air gravity and onshore Bouguer gravity (Olesen et al., 2010), with bathymetric contours at 500 m intervals shown on top. Euromargins 2003 OBS lines are marked by bold black lines, with OBS positions (circles) on Profile 8-03. White filled circles indicate OBSs returning data. Older surveys are shown as in Figure 1.

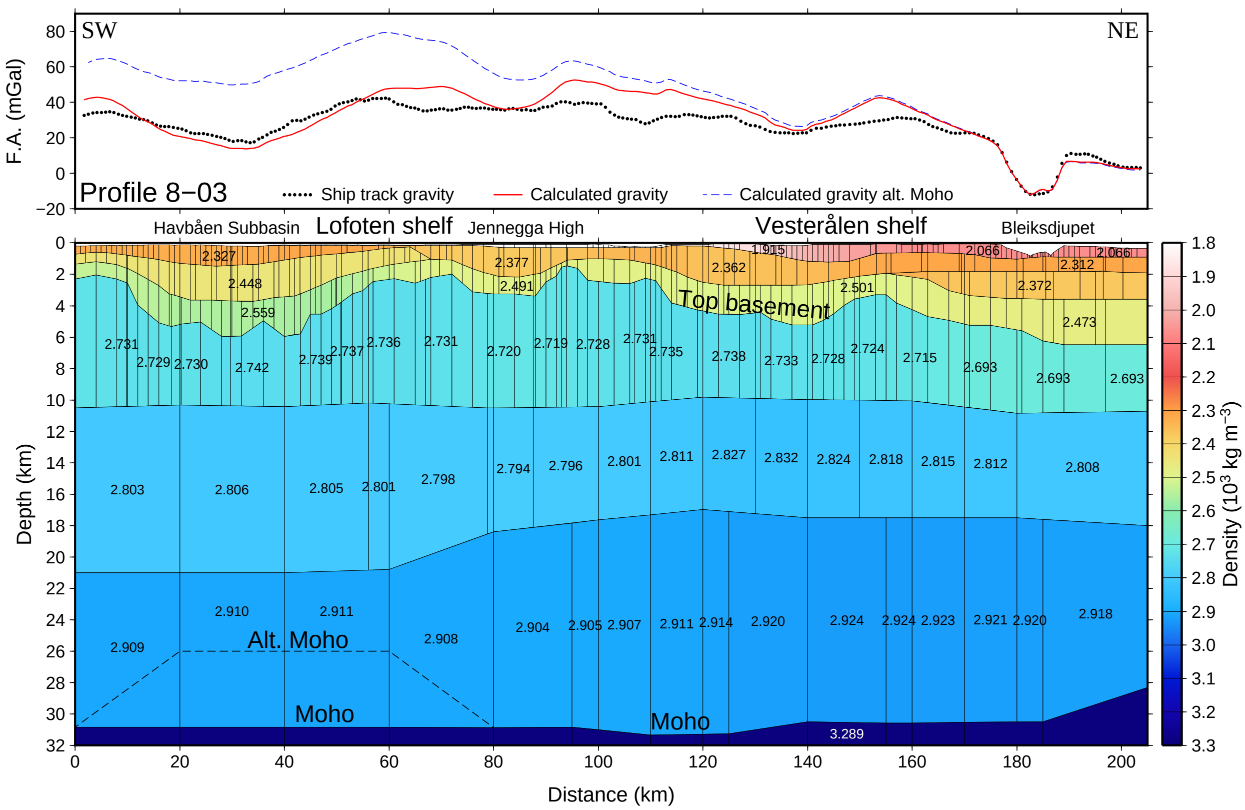

Figure 15: Gravity modeling of Profile 8-03, with densities derived from the average velocity within each trapezoid from the velocity model. The dashed line in the lower crust in the southwest shows the alternative Moho that was tested for. Typical densities are annotated in 10^3 kg m^{-3} on the model. Vertical exaggeration is 1:3. Top panel: Observed ship track Free-Air gravity and calculated model response.

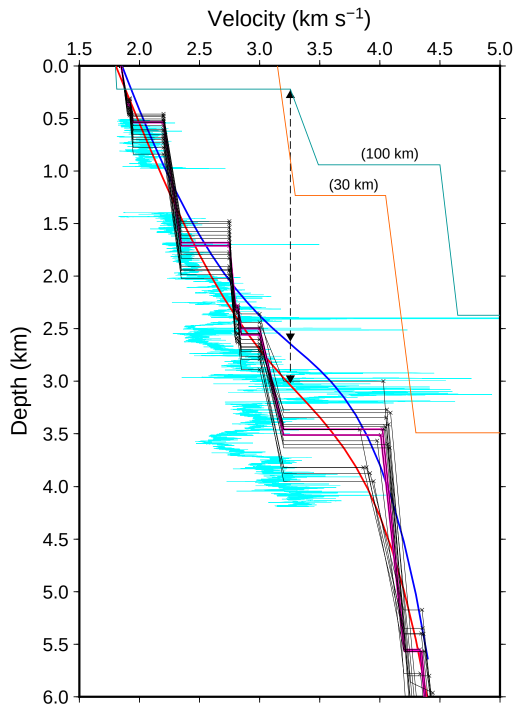

Figure 16: Velocity-depth 1D profiles sampled from OBS Profile B-98 of Mjelde et al. (2002) (staircase functions). The two velocity functions closest to the well tie are plotted in magenta. Bold red line shows the best polynomial fit to these curves. Blue polynomial fit line uses only the top-layer velocities (marked by x-symbols). The cyan line is the sonic log from Well 7216/11-1S located on-profile (Ryseth et al., 2003). Two 1D velocity profiles were sampled from the Profile 8-03 velocity model for comparison. The orange line is at 30 km model position within the Havbåen Subbasin, while the green line is at 100 km at the Jennegga High. The vertical dashed arrows show how the top layer velocities from the model can be compared to the reference curves in order to estimate the amount of erosion.

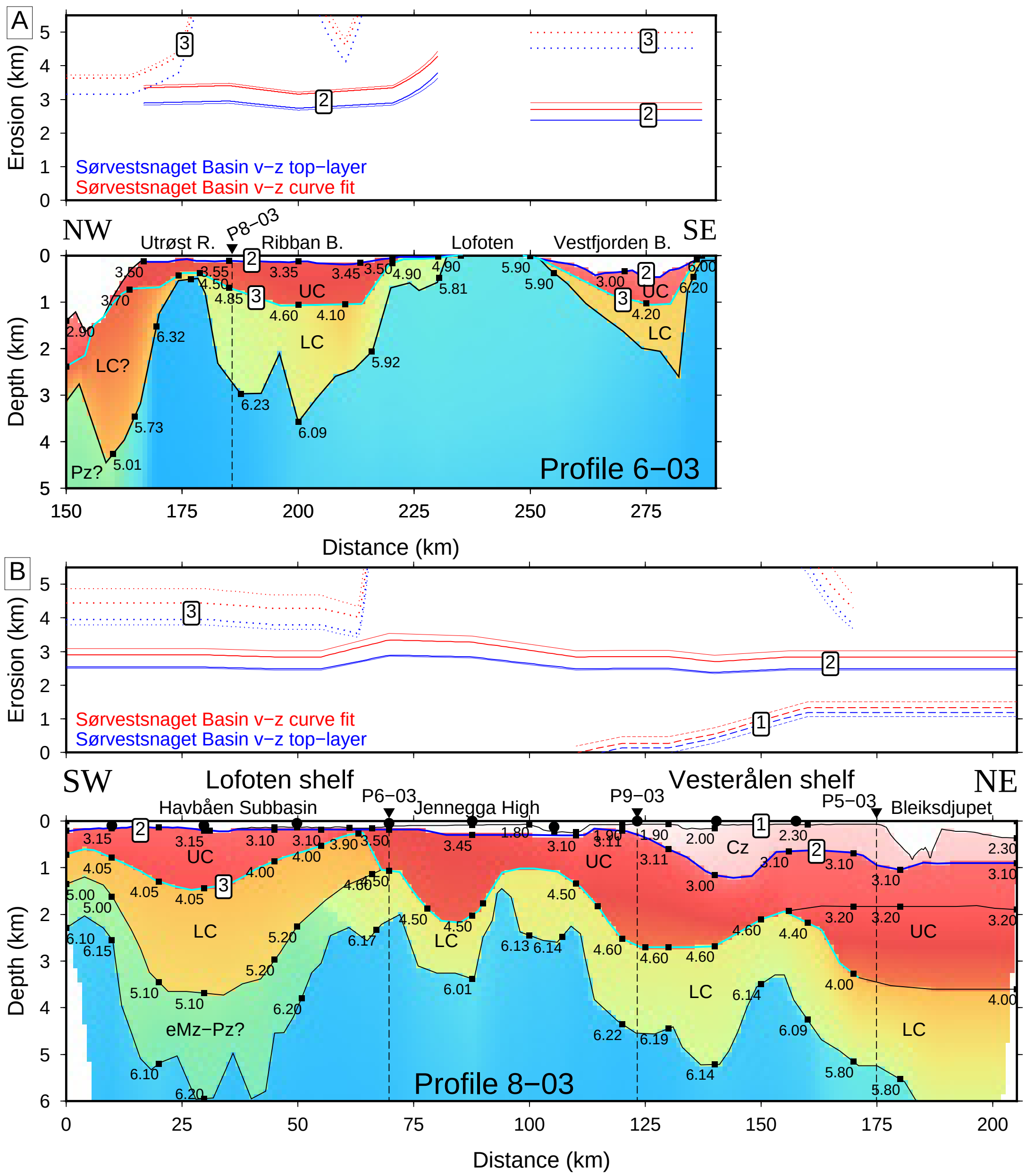

Figure 17: Gridded velocity models of the sedimentary section on the shelf. See Figure 10 for abbreviations. Top-layer velocity nodes are marked and annotated. The numbered levels shown on top of the velocity models mark where the different erosion estimates were made. Vertical exaggeration of velocity models is 1:10. The ties to other profiles are indicated by the inverted triangles and vertical dashed lines. In the erosion results panels, red refers to the best reference curve fit, while blue refers to the top-layer velocity curve fit shown in Fig. 16. Thinner lines below and above indicate minimum/maximum estimated from the velocity uncertainty of each sedimentary layer. A: Profile 6-03 (Breivik et al., 2017), with estimated erosion from two levels plotted above. B: Profile 8-03, with estimated erosion from three levels plotted above.